Multi-scale deformable layer reflection tomography and application to estimate base-salt geometry

---

A Dissertation

Presented to

the Faculty of the Department of Geosciences

University of Houston

In Partial Fulfillment

Of the Requirements for the Degree

Doctor of Philosophy

By

Fang Yuan

May 2015

Multi-scale deformable layer reflection tomography and application to estimate base-salt geometry

---

Fang Yuan

APPROVED:

Dr. Hua-wei Zhou, Chairman

Dr. Fred Hilterman

Dr. Aibing Li

Dr. Zhaobo(Joe) Meng

In-Depth Geophysical, Inc.

Dean, College of Natural Sciences and Mathematics

ACKNOWLEDGEMENTS

My deepest gratitude goes first and foremost to my dissertation advisor, Dr. Hua-wei Zhou, for his continuous guidance, encouragement and support in my study of geophysics at both Texas Tech University and University of Houston. Dr. Zhou's profound knowledge and deep insights in the field of geophysics enable me to learn a lot in my academic study and to complete this dissertation successfully. I would like to express my sincere gratitude for his kindness and generous help.

I also wish to express my heartfelt gratitude to Dr. Zhaobo (Joe) Meng, Dr. Bin Gong and Dr. Feng Qiao. Their brilliant ideas and constructive suggestions have proved immensely constructive, which helped my research and course work tremendously. I also thank In-Depth Geophysical Inc. for supporting my scholarship and providing computing resources.

I am also deeply grateful to my committee members: Dr. Fred Hilterman, Dr. Aibing Li, for taking time to serve as my committee members and their insights and numerous suggestions on my dissertation research. I thank to the Department of Earth and Atmosphere Sciences at University of Houston for the support of my Ph.D. study.

In addition, I am also very grateful to my friends and colleagues for their insightful discussions, which have further improved the quality of this dissertation. All of them deserve my full appreciation for their unselfish help.

Last, but certainly not least, I want to thank my parents, who help me go through the difficult times in my life. A special thanks to my husband Dr. Yong Ma and our daughter Iris; I appreciate the luck to have them during my Ph.D. study.

Multi-scale deformable layer reflection tomography and application to estimate base-salt geometry

---

An abstract of a Dissertation

Presented to

the Faculty of the Department of Geosciences

University of Houston

In Partial Fulfillment

Of the Requirements for the Degree

Doctor of Philosophy

By

Fang Yuan

May 2015

v

ABSTRACT

Salt-body delineation plays a critical role in oil-and-gas exploration in the Gulf of Mexico. Common practices for building a salt model rely on interpreting the top of salt first and then interpreting the base of salt on a migrated image. This process can be extremely time-consuming and resource intensive for a complex salt geometry and can be even more tedious in the presence of salt overhangs. The interpretation of base-salt geometry is often the most challenging part of the workflow, because salt base is typically poorly imaged due to limited illumination, which can be caused by the data acquisition, data quality, aperture, and choice of imaging algorithms. To facilitate the building of salt models, we propose a reflection layer tomography (RLT) that estimates the geometries of velocity interfaces by minimizing the kinematic errors measured on angle domain common image gathers. The goal for reflection layer tomography is to automatically and effectively estimate velocity interfaces such as salt boundary. This approach use common image gathers generated by accurate imaging algorithms such as reverse time migration. To mitigate the non-uniqueness of the tomographic inversion, we have further developed a multi-scale inversion. Compared with the single-scale RLT, the multi-scale RLT delivers superior results in delineating the base-salt geometry, as demonstrated by the synthetic examples. In addition, RLT has been extended to 3D for

more practical application. The synthetic results show that both migrated stack and common image gathers can be significantly improved using this approach.

TABLE OF CONTENTS

LIST OF FIGURES

Chapter 1:

Chapter 2:

Chapter 3:

Chapter 4:

LIST OF TABLES

LIST OF ABBREVIATIONS

ADCIGs	**Angle Domain Common Image Gathers**
BOS	**Base of Salt**
DLT	**Deformable Layer Tomography**
CIGs	**Common Image Gathers**
MVA	**Migration Velocity Analysis**
ODCIGs	**Offset Domain Common Image Gathers**
RLT	**Reflection Layer Tomography**
RTM	**Reverse Time Migration-**
TOS	**Top of Salt**

CHAPTER 1: INTRODUCTION

Seismic exploration relies on acquiring accurate subsurface properties, including subsurface structures and detailed velocity models. To accomplish this, pre-stack depth migration, for example, a two-way wave-equation based reverse time migration (RTM) can render superior structural images (Claerbout, 1985) of the subsurface, compared to other imaging methods, for example, Kirchhoff depth migration, beam migrations, and one-way wave equation migrations. As one of two-way pre-stack migration tools, RTM has been effectively implemented in a parallel computing environment to produce accurate images and angle gathers. However, the accuracy of RTM relies on an available and reliable velocity model, especially in complex geological areas. Various technologies have been developed over the past two decades to estimate such velocity models in both industry and academic settings.

Seismic tomography is a technique for estimating the Earth's 3D interior using seismic waves generated by earthquakes and explosions. The original method of tomographic inversion was proposed by Aki *et al.* (1974) for regional and global earthquake study. Global seismic tomography has been applied since the 1970s to help us understand sub-surface structure (Bois *et al.*, 1972; Aki and Lee, 1976; Aki *et al.*, 1977). The tomography velocity can be used to infer the depth of a mountain, the location of a

subducted slab, and even a hotspot location.

Exploration seismology has progressed greatly since the early 1990s (Woodward *et al.*, 2008). Bishop (1985) adapted the process of reflection seismology and proved that tomographic inversion is an effective way to accurately determine laterally varying velocity models. Strok (1992) extended reflection tomography to the postmigrated domain. Migration velocity analysis (MVA) is an image-domain process of estimating interval velocity by minimizes kinematic errors, which can be measured through common imaging gathers (CIGs), using a tomographic process (Symes, 1993). MVA is commonly performed in ray-based tomography in the oil and gas industry. Full-waveform inversion (Tarantola, 1984; Pratt, 1998; Ma *et al*., 2012) is a data-domain approach for estimating velocity models by minimizing the difference between recorded and modeled seismograms. In principle, Full-waveform inversion utilizes both kinematic and amplitude information and, therefore, can generate higher-resolution velocity models than kinematic-only tomography or MVA.

Salt basins (Figure 1.1), such as in the Gulf of Mexico, the West African Margin, and the Brazilian Margin, have been places to find the most prospective hydrocarbon deposits. Salt, as a low-density (2.16-2.20g/cm3) sedimentary rock, is easily driven entirely up-ward entirely by buoyant forces, leading to the formation of stratigraphic traps by moving and deforming surrounding sediments. Salt also acts as a seal, since it is

impermeable to hydrocarbons. For example, the Gulf Coast is trapped in a salt-related structure. The Jurassic-age salt body appears as domes with diapiric shapes, sheets covering much younger sediments in the Gulf of Mexico. The contrast between salt's high seismic wave velocity and that of sediments surrounding it leads to a strong conference reflection across the top of the salt dome, with no coherence energy below.

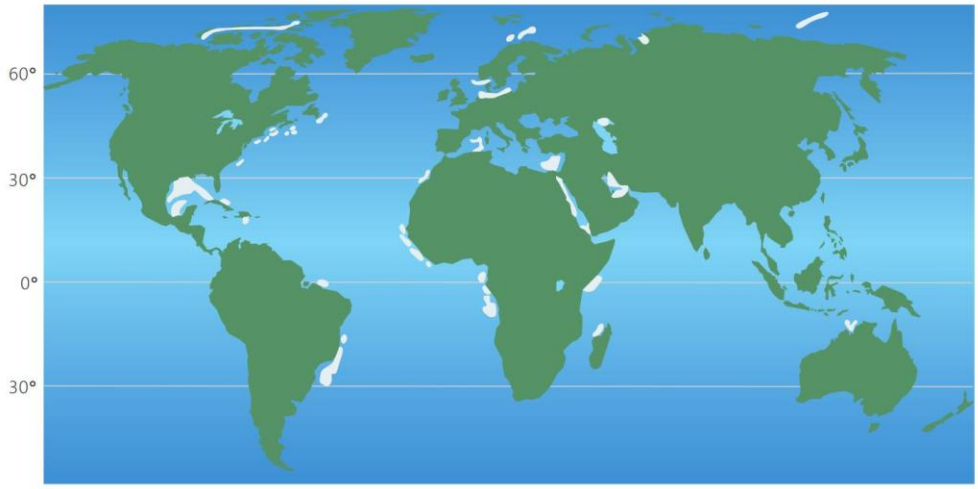

Figure 1.1: Worldwide offshore salt sheet distribution map (Sayers and Herron, 2007).

In 2005 and 2006, two workshops were held to discuss salt-related issues, emphasizing the challenges in salt-model imaging (Leveille *et al.*, 2005; Sava, 2006). With newly developed advanced imaging techniques, the top of salt (TOS) can often be effectively imaged (Figure 1.2) by pre-stack depth migration. Unfortunately, the salt base is much more difficult to image, and at the base of salt (BOS), the image usually suffers from poorer quality due to the lack of illumination or aperture. More importantly, the

subsalt structures are severely contaminated by artifacts caused mainly by using an inaccurate salt model for migration. Therefore, defining the salt body is an important element of the model building process for successful sub-salt imaging (Sayers and Herron, 2007; and Mosher *et al*., 2007).

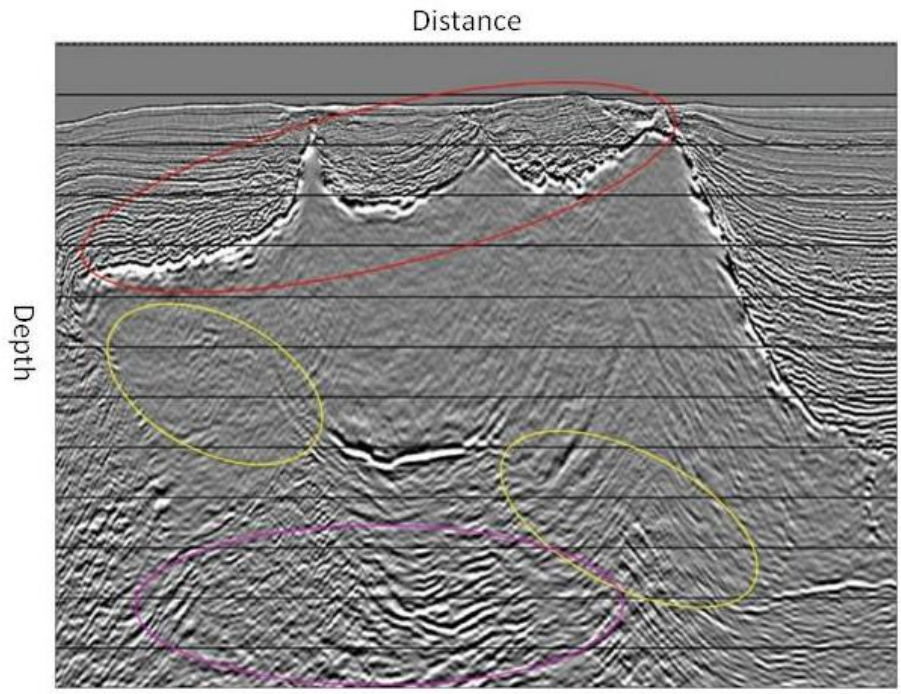

Figure 1.2**:** An example of sub-salt image (Leveille *et al.,* 2005). The red oval highlights the rugose top salt; the yellow ovals indicate the BOS; the subsalt energy in the pink oval shows crossing events and is of dubious value since the velocity model is not correct.

1.1 METHODS FOR SALT MODEL ESTIMATION

With many successful wells drilled around salt domes since the 1920s (Allaud and Martin, 1977), many methods have been developed to determine salt structures and to illuminate sub-salt reservoirs. The study of salt bodies has been an active topic for many years since the latter 1970s. However, as early as 1940s, Gardner (1949) determined salt-dome boundary using a detector buried inside a salt body. Lohmann (1979) illustrated characteristics that distinguish a salt body from other structure types. May and Covey (1983) discussed the possibility of imaging an overhanging salt dome using inverse modeling by ray methods. Lin (1991) applied wave field imaging and processing techniques to model and image salt dome structures. With the development of MVA in the industry, the tomography based on residual moveouts (RMOs) in prestack depth migration gathers is the standard method by which to update the velocity model (Stork, 1992; Wang, *et al.*, 1995; Zhou *et al.*, 2001).

In the oil-and-gas industry, building an accurate model of a salt body remains a great challenge. Taking the BP2004 2D salt model (Figure 1.3a) as an example, the standard industrial workflow for imaging salt areas consists of several steps of interpretation and velocity building:

(1) Estimate the background velocity model (Figure 1.3b) using existing model building techniques, including compaction trends, velocity analysis, and conventional traveltime tomography.

(2) Use new advanced imaging techniques, such as RTM, to obtain an image with the background model and then pick the top of salt (TOS) based on the migrated image (Figure 1.3c).

(3) Flood the salt (Figure 1.3d) from the top salt all the way to the bottom of the velocity model.

(4) Perform a new prestack depth migration with the salt-flood model and then pick the BOS based on the salt-flood image (Figure 1.3e).

(5) Update the salt flank geometry according to the picked TOS and BOS after several iterations of salt flood and RTM (Figure 1.3f and Figure 1.3g).

(6) Combine the salt body together with the background model to achieve the final salt model (Figure 1.3h), and apply a final migration (Figure 1.3i) using this final model.

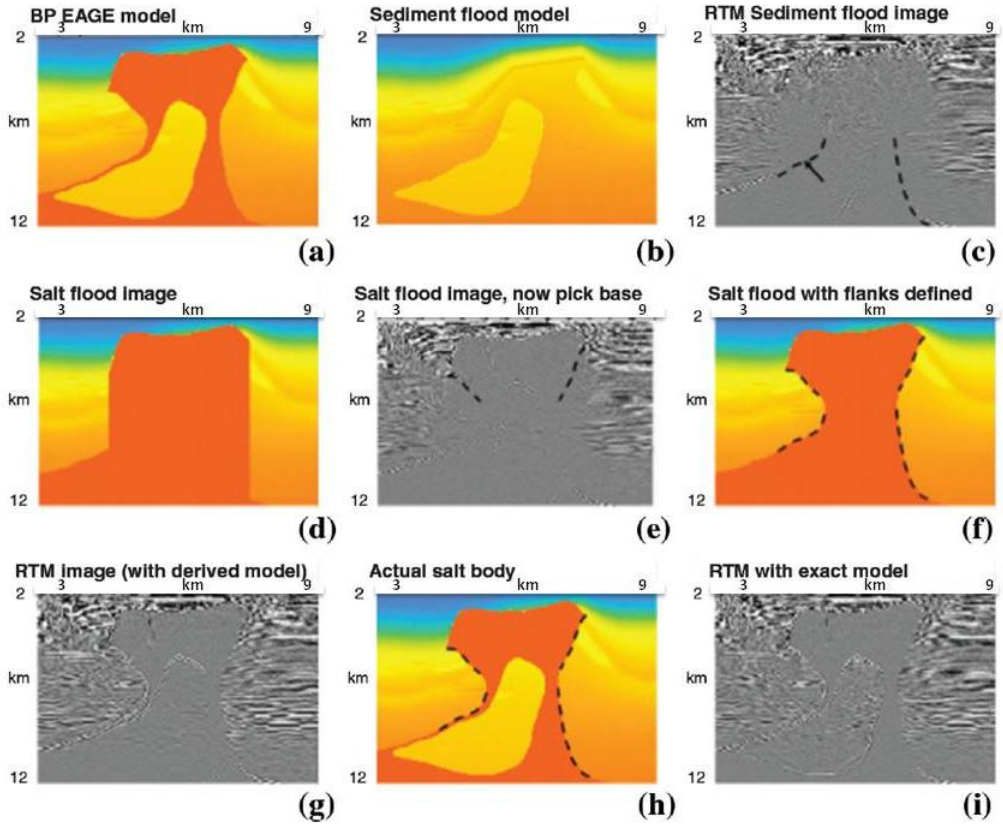

Figure 1.3: (a) Portion of the BP 2D sale model used to generate synthetic data. (b) The salt body has been removed to create a background model for commencement of a salt model building work flow. (c) Migration using the sediment only velocity field produces an image from which the top salt and some salt flank horizons can be picked. (d) The salt picks are inserted into the velocity model, and values of salt velocity "flooded" vertically below the picked top and flank salt boundaries. (e) From the salt flood migration, the BOS horizon is picked. (f) The salt body geometry is updated based on the available picks to create the salt geobody. (g) Migration using the derived salt model. (h) Correct BP salt for comparison. (i) Migration using the correct salt model for comparison (Leveille et al., 2011).

1.2 CHALLENGES IN CURRENT APPROACH FOR SALT-MODEL ESTIMATION

The above standard salt-model-building workflow indicates that the salt model building is an iterative process that truly integrates salt interpretation and depth imaging. Significant human interaction is involved to pick salt surfaces. About 70% of a typical depth-image project is accounted for by salt interpretation (Reasnor, 2007), making the salt-body estimation extremely time consuming and resource intensive.

More automatic model building methods, such as conventional tomography or MVA, focus on determining sediment velocities rather than on estimating the salt model. In addition, the solution of tomographic inversion is often underdetermined. Model parameterization is a fundamental issue in seismic tomography. Deformable layer tomography (DLT) represents the velocity with thickness varying layers, which is based on stratigraphic interpretation (Zhou, 2006). DLT can estimate a good near-surface velocity model (Liu, 2010) by using parameters of layer-based model. Unlike the most common cell or grid tomographic methods widely used in MVA, this method suffers less from the smear artifacts. Hence DLT can directly map pitchout features such as basin boundaries and undulations of velocity discontinuities. In order to combine the advantages of MVA with DLT, a new method RLT is developed to automatically delineate the BOS geometry.

1.3 DISSERTATION OVERVIEW

In this thesis, a method of RLT is proposed to estimate P-wave velocity interface. This method takes advantage of both conventional reflection tomography and DLT, and works by iteratively updating velocities and reflector positions along ray path of source-receiver pairs minimize RMOs.

The motivation of this study is to utilize the depth residual information in common image gathers, which is sensitive to macro velocity model. Moreover, the study of influence of coupling and uncoupling between velocity interfaces and geometry of reflectors can give us a better understanding of how to effectively parameterize models in inversion. It also offers an opportunity to adopt geologic constraints, for example, determining reflector location from well log data.

The novelty of this study is that RLT updates reflection interfaces during the migration velocity analysis, where the interfaces are highly constrained layer-based structures and the background velocity is a less structurally constrained, more data-driven grid-based representation. This differs from most geophysical inversion methods that update only the background velocity model. In addition, this method allows the thickness of layer to be reduced to zero in the model and can conveniently incorporate the known geologic information from previous work into the starting model.

In order to reduce the nonuniqueness in ill-posed inversion problems and to improve

the stability of reflection tomography, I also propose to extend this RLT method to update reflector interfaces during tomographic iterations in a multi-scale sense. Based on the experience from multi-scale DLT (Zhou, 2006), the multi-scale RLT can also be used to improve the resolution of thickness-varying layer models and efficiently determine the best-data-fit depth and thickness of these layers.

One particular problem I want to tackle in my thesis is to estimate the base of the salt model and thereby to improve the subsalt imaging. The geometry of layer boundaries is updated by inversion at each node along the layer interface. Depth perturbations at layer nodes are the unknown parameters. All synthetic and field data are designed as shallow water. In addition, a multi-scale tomography technique (Zhou, 2003) is used in the inversion to reduce the difficulties caused by uneven distribution of complex ray paths. In this dissertation, multi-scale is applied to improve the ray coverage and helps the inversion converge to the global minimum variables during the inversion process.

1.4 DISSERTATION OUTLINE

The main content of this thesis covers the five chapters as follows:

In Chapter 1, it gives the general introduction to this thesis.

In Chapter 2, a new method of RLT is developed to update velocity interfaces through the analysis on migration velocity. One particular problem that can be solved through this

study is the estimation or identification of velocity interface, especially the BOS, which is usually a relatively challenging issue. In this chapter, the effectiveness of RLT method in estimating or identifying the BOS geometry is demonstrated in details.

In Chapter 3, a multi-scale RLT is proposed to reduce the nonuniqueness due to uneven and poor ray coverage and to improve the inversion quality. In this chapter, both the synthetic data and initial model shown in Chapter 2 are used to demonstrate significant improvement of multi-scale RLT.

In Chapter 4, RLT is extended to the 3D case to make it applicable to real problem. A more realistic 3D marine survey is created to check the reality of this method.

In Chapter 5, this thesis is summarized and future work is proposed.

CHAPTER 2: REFLECTION LAYER TOMOGRAPHY

2.1 OVERVIEW

Tomography, as a specific type of inversion process, was formally described by Backus and Gillbert using geophysical observation in 1968. In exploration seismology, we rarely have sufficient data to determine unique solutions. A series of measurements of traveltime or waveforms associated with seismic refractions, reflections, and transmissions are used to build a subsurface velocity model. There are two main types of seismic data used in the invert velocity model: traveltime data and waveform data. Although waveform data can reconstruct a higher resolution velocity than traveltime tomography, travel tomography is more robust and has faster computation ability than waveform data.

In industry, prestack depth migration (PSDM) domain ray-based tomography has been the current standard model building tool for seismic depth imaging since the late 1990s (Stock, 1992; Wang *et al.*, 1995). Moreover, the standard model resolution has been increased to a few hundred meters contributed by high-quality picks of RMOs.

In practice, there are two main model parameters that can be used for the velocity model: one is the layer-based approach and the other is the grid-based approach. Highly

constrained and interpreted layered tomography was developed to update data velocity interface geometry using primarily reflection data (Bishop *et al.*, 1985; Guiziou *et al.*, 1996; Kosloff *et al*., 1996). Geological features, such as weathering zones, stratigraphic units, lithologic boundaries, and salt bodies, can be used to easily represent layer tomography (Zhou, 2006). The layer-based model has the potential to constrain the geometry of velocity interfaces in areas with prior knowledge of velocity values and subsurface geometry information. The grid-based approach is commonly adopted in less constrained environments; it is a more data-driven approach used to uncover the subtle variations associated with velocity regimes decoupled from sedimentation.

In this chapter, I briefly describe a type of layer based tomography and conventional reflection tomography. I develop the algorithm of RLT, which combines the advantages of layer based DLT and conventional grid based reflection tomography. The analytical kernels are derived in terms of traveltime based on geometric reflection. By solving an inverse problem, RLT can iteratively update velocity using RMOs in ADCIGs. In the end, I show a 2D synthetic example to demonstrate RLT method.

2.2 DEFORMABLE-LAYER TOMOGRAOHY

DLT, as a type of layer based tomography, focuses on constraining the geometry of velocity interfaces. Since the model is based on layered parameterization, DLT can

conveniently represent many important geological features, including basin boundaries and velocity discontinuities, by layers of varying thickness. With knowledge of the velocity range, DLT directly inverts for velocity interfaces. To reduce depth and velocity ambiguities (Bickel, 1990; Lines, 1993), DLT assumes a constant velocity in each layer. As shown in Figure 2.1, a number of control points are distributed on velocity interface. During the inversion process, the depth of control points will change and velocity interfaces are updated. Layer based tomography is also more effective to compute than grid-based tomography in mitigating smearing artifacts using a minimum number of model variables.

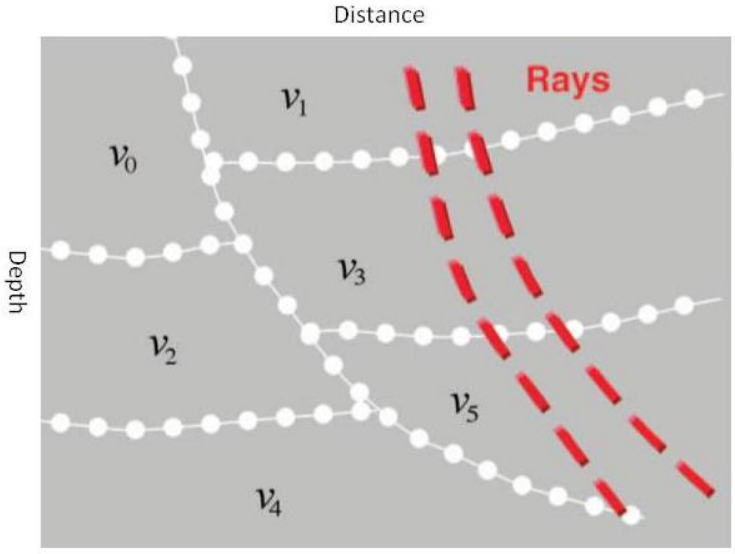

Figure 2.1: Layered model with constant velocity in each layer. Layer tomography focuses on determining the geometry of velocity interfaces. The white dots are the control points, which will be updated during inversion. When velocity values are known, the interface geometry is often constrainable even with nearly parallel rays (Zhou, 2006).

Similar to the formulations drawn from Zelt and Smith (1992), Kosloff *et al.* (1996), and Wang (1999), the Frechet kernels for DLT can be written as follows (Zhou, 2006):

$$\Delta t_i = \sum_j^J k\_s_{ij} ds_j + \sum_l^L k\_z_{il} dz_l \qquad (2.1)$$

Where Δt_i denotes the traveltime residual of the *i*th ray. The first term on the right-hand side of the equation 2.1 is a dot product of the slowness kernel k_s_{ij} and the slowness perturbation Δs_j, for the *ith* ray in the *jth* cell; the second term is a dot product of the interface kernel k_z_{il} and the interface perturbation Δz_l for the *ith* ray in the *lth* cell. The objective of DLT is to give a reference model and estimate Δs_j and Δz_l by minimizing traveltime residuals Δt_i.

A typical DLT workflow consists of the following three steps. Step1: initial model building. The model is set up using a set of layers of known velocity values or ranges from previous works. Constant velocity is assumed for each layer to help reduce the number of inversion unknowns and keep the velocity function simple. Step 2: ray tracing and traveltime computation. Rays trace through the model to calculate the traveltimes. For one ray each time, the model's partial derivatives related to the depth perturbation of corner nodes on the interface are evaluated and calculated. Step 3: traveltime fitting. During the inversion, our purpose is to minimize the misfit travel-time residual, which is difference between the observed traveltime and the predicted travel-time. If the

travel-time residual misfit is small, we consider the new model to be a viable solution. The difference from conventional reflection tomography, the reflection traveltime of DLT does not come from migrated image.

2.3 CONVENTIONAL REFLECTION TOMOGRAPHY

In the oil industry, ray-based, pre-stacked depth migration domain grid tomography is widely applied in performing migration velocity analysis (MVA). Velocity estimation and imaging are interlaced processes. Migration is an essential tool for velocity analysis because it studies the degree of focus in the output images and event flatness in common image gathers (CIGs). The fundamental principle of MVA is that correct velocity must accurately explain the relative time delay between subsurface reflections of the same interface (Biondi, 2006). Velocity perturbation is analyzed in the post-migration domain, which is more robustly performed than in the data domain before migration.

The deviation from flatness measured in the migrated CIGs can be quantitatively related to kinematic errors accumulated by the wave propagation through an inaccurate migration-velocity model (Biondi and Symes 2004; Biondi and Tisserant 2004), and the kinematic errors can be inverted in velocity errors by a tomographic method. The depth variation of reflectors along common image gather is residual moveout (RMO). Standard industry grid tomography produces velocity to flat RMO in the common imaging gather

model.

Using Fermat's principle, Figure 2.2 illustrates the effect of small reflection positon variation on traveltime (Δt):

$$\Delta t = \frac{2\cos\theta\cos\phi\Delta z}{v} \tag{2.2}$$

Where θ is the incident angle, ϕ is the dipping angle, v is the local velocity at the reflector, and Δz is the vertical perturbation perpendicular.

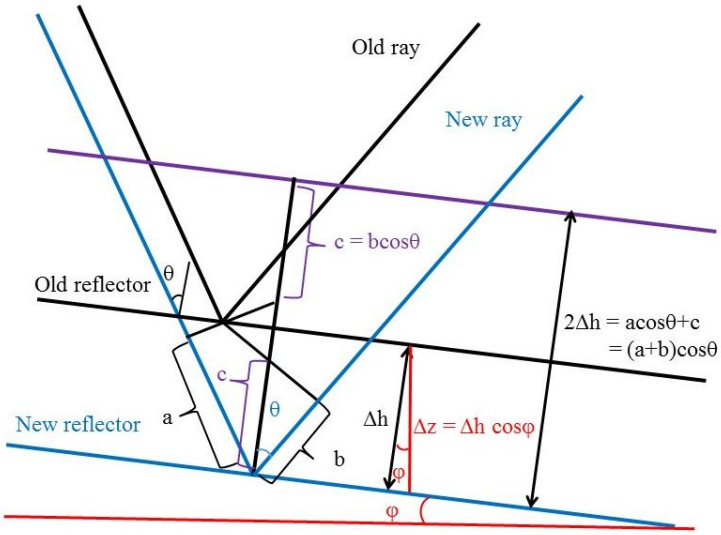

Figure 2.2: A Demonstration of the extra travelling distance by a ray due to an infinitesimal relfector vertical perturbation dz. The extra traveltime is this distance divided by the local velocity (modified from Stork and Clayton, 1991).

Thus, the connection between RMO Δz and velocity perturbation is as follows:

$$\Delta z = L\Delta s = \sum_{i}^{I}\left(\frac{\partial t_i}{\partial s_i}\Delta s_i\right)\frac{v}{2\cos\theta\cos\phi} \tag{2.3}$$

Where L contains the geometry and background model term, i indicates a node on the model grid, θ is the angle of incidence for the reflector at the current CDP location, ϕ is the reflector dip, v is the effective velocity at this reflector, and $\partial t/\partial s_i$ is the Frechet derivative, measuring the change in traveltime with respect to the slowness change in the i^{th} node.

Figure 2.3 illustrates the standard grid reflection tomography workflow in the oil industry. Step 1: create a pre-stack depth migration on a current best-estimated initial velocity model to obtain RMOs from pre-stack migrated gathers. Step 2: automatically pick dips from the stack cube and RMOs from pre-stack depth migration gathers. Step 3: trace the ray paths for each offset/angle pick. Step 4: form tomographic equations build a ray-trace linear system of tomographic updating equations and perform tomography inversion. This procedure is run multiple times until the process converges on an optimized velocity model by flattening the RMO and obtaining a velocity model with increasing detail and accuracy. Residual moveout will be linearly distributed along ray paths to form tomographic equations.

By solving the tomographic equations, we can obtain smooth velocity updates.

However, as I mentioned earlier, this method does not handle velocity interfaces, such as salt boundary.

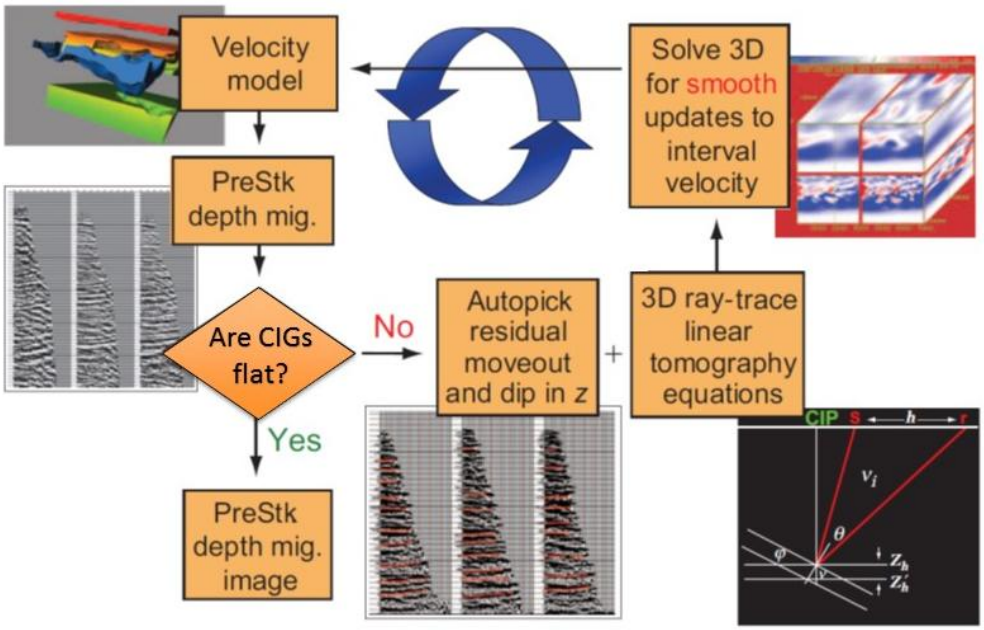

Figure 2.3: Conventional reflection traveltime tomography workflow (Woodward *et al.*, 2008).

2.4 METHOD OF RLT

Based on the salt structure distribution, a layer-based model can express its anomalies using a minimum number of model variables. It is easy to implement and can be efficient for computation. Velocity perturbation is analyzed in the post-migration domain, and this analysis is more robustly performed than in the data domain before migration.

The reason for maintaining constant velocity in RLT is to maintain constraining power and to reduce depth and velocity ambiguity (Bickel, 1990). RLT describes an alternate approach to velocity determination based on migration velocity analysis. It represents the velocity model by reflection layers, and it updates layer depth from an initial model. This section describes the theory behind RLT.

2.4.1 RTM Angle Domain Common Image Gather

Offset Domain Common Image Gathers (ODCIGs), as one type of CIGs, are widely used in MVA. However, it is well known that ODCIGs suffer from multi-pathing in complex velocity model, such as, salt domes, gas clouds, low/high velocity zones. Unlike ODCIGs, angle domain common image gathers (ADCIGs) organize energy in a range of reflection angles (Xu *et al.*, 2001; Meng and Bleistein, 2001). Although multiple source-receiver ray pairs (Figure 2.4) can correspond to the common surface offset, the reflection angles for these different specular rays are different at the subsurface image

point, indicating that each event on ADCIGs is unique for one subsurface point. Therefore, ADCIGs do not suffer from multi-pathing, and can thus provide more reliable and stable RMOs for tomography to build more accurate subsurface models.

Compared to ray-based Kirchhoff, wave-equation based methods (for example, RTM) are not only superior in depth image quality, but they are also robust in velocity model building. RTM solves two-way wave equations (Baysal *et al.*, 1983; McMechan, 1983; Whitmore, 1983) and thus yields higher accuracy in modeling complex wave propagation including turning waves and multiply bounced waves, such as prism waves (Jones, 2007). RTM can image steep-dip reflectors and is capable of imaging salt shadow zones, improving event termination against salt flanks, and providing superior images for rugose TOS and the more challenging BOS. With some manageable costs, RTM can produce ADCIGs, which indicate model errors in a more robust manner than ODCIGs, which are often generated by traditional Kirchhoff migration (Yoon *et al.*, 2008; Liu and Wang, 2008).

ADCIGs can be obtained by a variety of ray-based or wave-equation-based prestack migration methods, including Kirchhoff depth migration, beam migration, one-way wave-equation migration, or RTM. Among all these methods, RTM, implemented by a two-way wave equation, provides the most accurate and complete images because it imposes no dip limitation and can simulate wave propagation in complex media. In this

paper, we adopt RTM to compute ADCIGs.

In conventional RTM image can be obtained by cross-correlating the source and receiver wavefields at each subsurface image point. As shown in Figure 2.5, p_S and p_R indicates the propagating directions of a source wavefield and a receiver wavefield, respectively, at one image point *M*. A Poynting-vector-based method (Yoon and Marfurt, 2006) can be used to compute the directions $\mathbf{p}_S$ and $\mathbf{p}_R$, which together with the normal direction **n** at *M* define, for this pair of source and receiver wavefileds, the reflection angle θ and the azimuth angle φ. In fact, provided many shots, different source and receiver wavefields can illuminate this image point from different reflection angles and form a set of images, which can be binned as a function of the reflection angle to form ADCIGs. The conventional RTM image is the summation of ADCIGs for all the reflection angles.

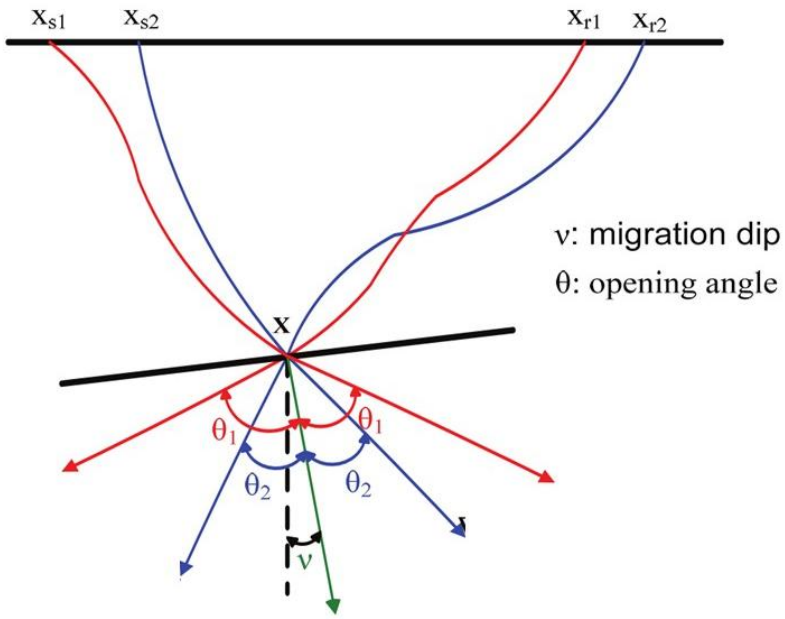

Figure 2.4: A dipping reflector x with two sets of specular rays from the source-receiver pairs. They have the same offset but different opening angles at depth (Bleistein and Gray, 2002).

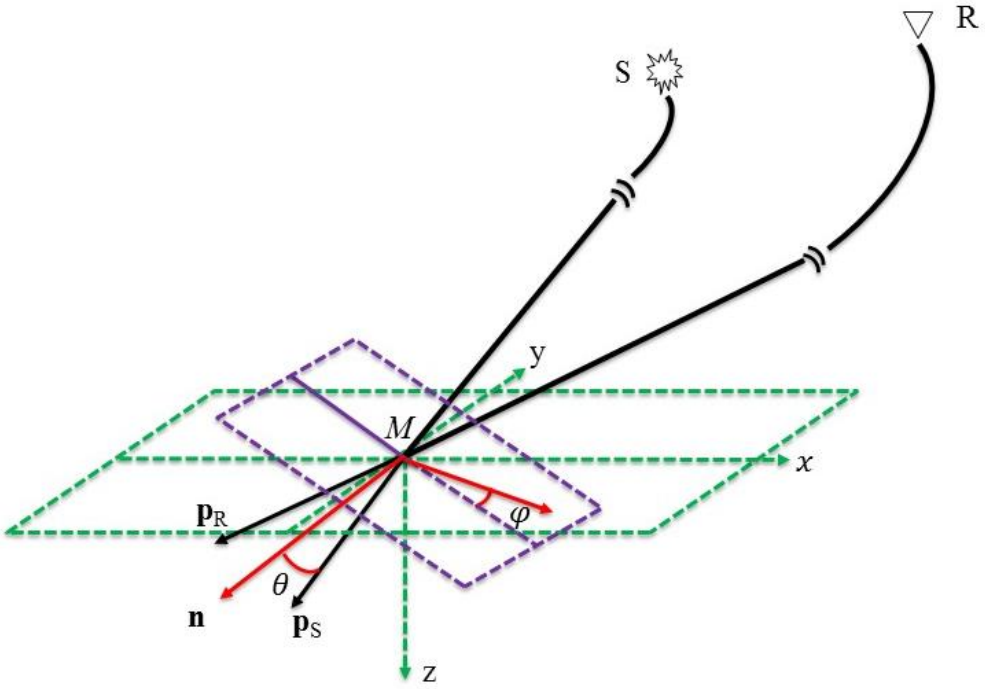

Figure 2.5: A schematic illustration of common-angle gathers from RTM. At a subsurface point M, $\mathbf{p}_S$ and $\mathbf{p}_R$ indicate the propagating directions of two wavefields originated from a source S and a receiver R, respectively. $\mathbf{p}_S$, $\mathbf{p}_R$ and the normal direction **n** at the image point *M*, define the reflection angle θ and the azimuth angle φ., which correspond to the source and receiver wavefields. Zero-lag crosscorrelation of the source and receiver wavefields provides a RTM image at *M*, which in fact is a function of θ and φ. For the same image point *M*, many shots can illuminate it form different directions, thereby forming a set of images associated with different reflection angles. In this paper, we form ADCIGs by binning all the RTM images at *M* as a function of the reflection angle, $I_M(\theta)$.

2.4.2 Model Parameterization

Tomographic velocity analysis starts with model parameterization. Blocky (or layered), gridded, tessellated, and B-splined models are commonly used in exploration seismology. The grid based velocity model, as the most widely used model representation scheme in tomography or MVA, is resolved given a sufficient number of intersecting rays at each grid. The layer based model has the potential to constrain the geometry of velocity interfaces in geological features such as salt body, stratigraphic units, etc. Layer-based models rely heavily on interpretation results and are useful in poor data quality areas where strong geological constraints are necessary.

RLT takes advantage of two model parameters. The RLT model (Figure 2.6c) consists of two models: the grid based velocity model (Figure 2.6a) and a layer based interface model (Figure 2.6b). During the RLT inversion, the layered interface model is updated; then it is converted to the gridded velocity model for modeling and migration purposes.

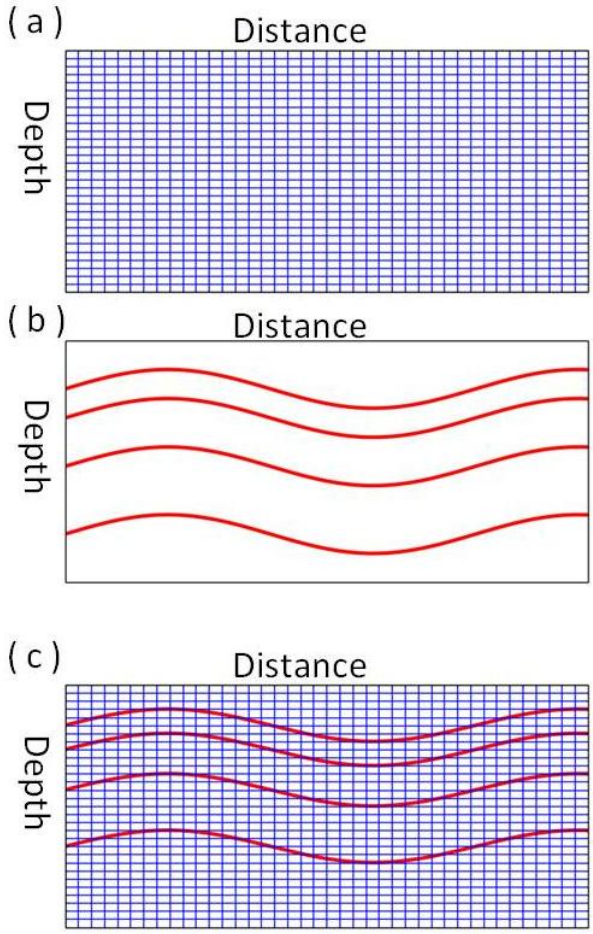

Figure 2.6: (a) A gridded velocity model. Each blue rectangle has its velocity value. (b) A layered interface model. Red curves are velocity interfaces. (c) RLT model in 2D case.

2.4.3 Inverse Problem

The purpose of my study is to determine the geometry of the velocity interface, especially the salt boundary. The depth of each layer with constant velocity of the model can be obtained based on the best fit to the observed traveltimes. Both horizontal and vertical resolution of the obtained models can be controlled through the process of model parameterization. As we will show later, by carefully selecting parameters, we can derive geologically plausible velocity models, which will reveal the complex geology in the study area.

As another image-domain tomographic method, RLT aims to update the velocity interfaces by minimizing RMO in the migrated ADCIGs. We follow the way in conventional tomography to derive the inversion kernel for RLT. In RLT, we connect RMO and the interface model using

$$\Delta z = \sum_{i}^{I} \left(\frac{\partial t_i}{\partial d_i} \Delta h_i\right) \frac{v}{2\cos\theta\cos\phi} \qquad (2.4)$$

d_j is the depth change of the j^{th} grid of the interface model, $\partial t_k / \partial d_j$ is the Frechet derivative for RLT.

Figure 2.7 depicts that a ray intersects with a velocity interface, which consists of a set of control points. In our interface model parameterization, each interface control point

provides velocity information above and below the interface. From a geometric relationship, we can obtained

$$\frac{\partial t_i}{\partial d_j} = \left(\frac{1}{V_j^{below}}\cos\alpha - \frac{1}{V_j^{above}}\cos\beta\right)\frac{\left\|x - x_j\right\|}{\left\|x_j - x_{j-1}\right\|} \tag{2.5}$$

where x is the intersecting horizontal coordinate between the ray and the interface, x_j and x_{j-1} are two grids bracketing x, $\left\|x - x_j\right\|$ stands for the distance between x and x_j, the ray propagating angles α and β below and above the interface obey Snell's law, V_j^{below} and V_j^{below} are velocities below and above the interface at the j*th* grid, respectively.

The image misfit (ΔZ) is used to update the interval velocity model in an effect to minimize the misfit quantity.

$$\Delta z = z_{far-angle} - z_{near-angle} \tag{2.6}$$

where $Z_{far\text{-}offset}$ and $Z_{near\text{-}angle}$ indicate the migrated reflector depths in postmigrated ADCIGs at large-angle and small-angle locations, respectively

We can rewrite the RLT system in equation 2.5 as a matrix-vector format

$$\begin{cases} \mathbf{A}\Delta\mathbf{d} = \Delta\mathbf{t} \\ \mathbf{R}\Delta\mathbf{d} = 0 \end{cases}, \tag{2.7}$$

where $\Delta t_i = \Delta z_j / v * \cos\theta * \cos\varphi$, $A_{ij} = \partial t_i / \partial d_j$ and **R** is a regularization operator. Then the goal of RLT is to solve this linear system of equations for velocity interface perturbations $\Delta\mathbf{d}$. Like most geophysical inverse problems, this RLT problem in equation 2.7 is also not well determined. We use a nonlinear preconditioned conjugate-gradient

method to solve this problem by minimizing the misfit function $\left\|\mathbf{A}\Delta\mathbf{h}-\Delta\mathbf{t}\right\|^2$, where $\left\|\bullet\right\|^2$ means an L2 norm.

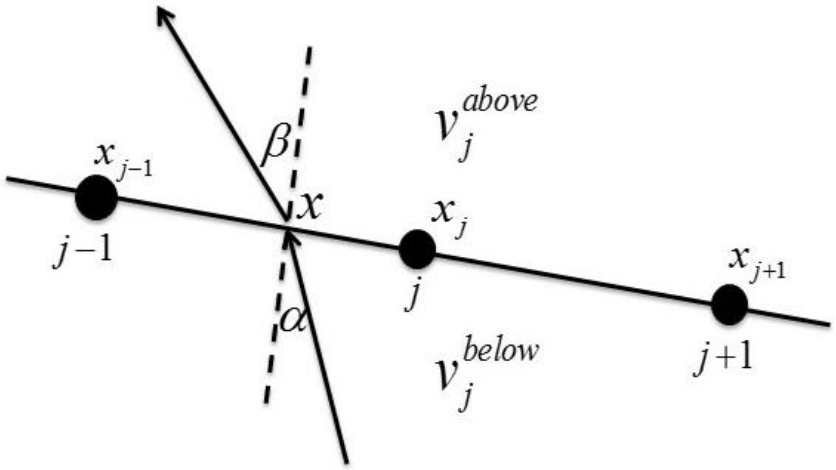

Figure 2.7: Schematic illustration of ray intersecting with an interface. The interface is represented by a set of control points, and each control point provides information about velocities above and below the interface, V_j^{below} and V_j^{above}, respectively. The ray obeys Snell's law when passing through the interface.

2.4.4 Implementation

In RLT, the velocity estimation and RTM imaging are interlaced processes. The flatness of RTM ADCIGs and the continuity of the stack image is the criteria for evaluating a velocity model. With a given initial velocity model, the workflow (Figure 2.8) of RLT consists of the following steps.

1) Generate ADCIGs using RTM.

2) Automatically pick RMOs on the ADCIGs.

3) Solve a linear system of equations to invert for the depth perturbation at each control point and update the interface model.

4) Convert the updated interface model to the gridded velocity model and run RTM to produce new ADCIGs

5) Check for image quality and flatness of ADCIGs. Exit the loop if the model provides satisfactory images and ADCIGs.

Although the main work of this study is to develop the new tomography method, I did finite-difference forward modeling on synthetic true model to generate input data. I also went through seismic data processing steps to obtain the RMOs from RTM ADCIGs for RLT.

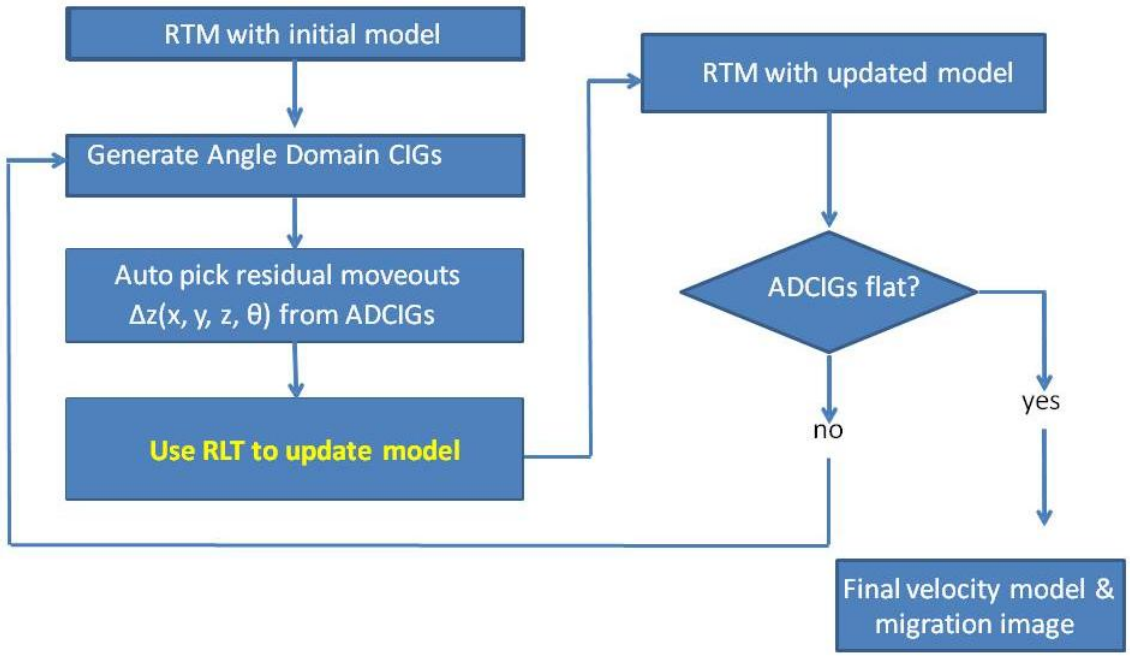

Figure 2.8: A typical work flow for reflection layer tomography.

2.5 SYNTHETIC EXAMPLE

A 2D synthetic test is designed to demonstrate the validity of RLT. Synthetic examples give the benefits of knowing the true model; hence it provides an objective comparison of different methods. Finite difference forward modeling was applied on synthetic true model to generate data for migration purpose.

A typical survey geometry is designed to generate synthetic common shot gathers using finite difference forward modeling, which is different from the RTM engine. The details of this acquisition geometry are shown in Table 2.1. A total of 321 shots are located in the survey area, with a maximum offset of 8 km. Shot and receiver intervals are 50m and 25m, respectively. The end-on spread acquisition is applied, and Figure 2.9 shows the relationship between one shot and its receivers.

The salt body in the true-velocity model (Figure 2.10) has rugose top, which commonly exists in Gulf of Mexico. For simplicity but without losing generality, 1D background velocity was built as the sediment. The salt body with a velocity 4.5 km/s embedded in a 1D gradient background velocity ranging from 1.5 km/s to 3.5 km/s. Six horizontal reflectors located beneath the salt will provide reflection signals for the inversion.

RTM, as an advanced imaging technique, is applied on the initial model to generate a migrated image as a critical standard during the model updated. With the correct model, RTM provides a correct image (Figure 2.11) of the subsalt. Every reflector is superb

focused and located these events at the right positions.

The base of salt of the initial velocity model (Figure 2.12) is significantly deviated from the true BOS location, which is plotted by the dashed curve. The RTM image (Figure 2.13) with the initial velocity model shows severe defocus and discontinuity below the center part of the salt, indicating the artifacts in the velocity destruction and the incorrect salt structure. Here, we assume the sediment velocity and the geometry of TOS are known. Figure 2.14 displays ADCIGs of initial velocity model generated by RTM. They correspond to the migrated stack in Figure 2.13 by showing the curved events in the defocused subsalt areas. The maximum angle of each gather is 50°, with an increment of 2°.

Significant RMOs can be obtained from ADCIGs of initial model, especially in subsalt areas. The tomographic inversion is carried out iteratively by minimizing these RMOs (Figure 2.14) to recover the BOS geometry. Starting from the initial model in Figure 2.12, the BOS of the first iteration (Figure 2.15) moves to the right direction; the second iteration (Figure 2.16) continues to improve the BOS; however, from the third iteration (Figure 2.17), the BOS starts to become over-corrected at some locations; the fourth iteration (Figure 2.18) tries to bring some of the over-corrected BOS back towards the right direction. Compared to the true model in Figure 2.10, the RLT solution in the fourth iteration shows that the general BOS boundary features are recovered.

In Figure 2.19, the migrated RTM ADCIGs for the model after four iterations of single-scale RLT updates also verify these improvements. As we can see, most of the reflection events beneath the salt become flatter. Still, obvious RMOs exits below the steep dip salt flanks, which are highlighted by the arrow and circles in Figure 2.19. The model (Figure 2.18) and the corresponding RTM image (Figure 2.19) and ADCIGs (Figure 2.20) are not quite satisfactory, indicating room for further improvement.

Table 2.1: Acquisition geometer of 2D synthetic survey.

Number of shots	321
Number of receivers	321
Shot interval	50 m
Receiver interval	25 m
CDP interval	12.5 m
Maximum offset	8,000 m
Acquisition time	8 s
Sample rate	4 ms

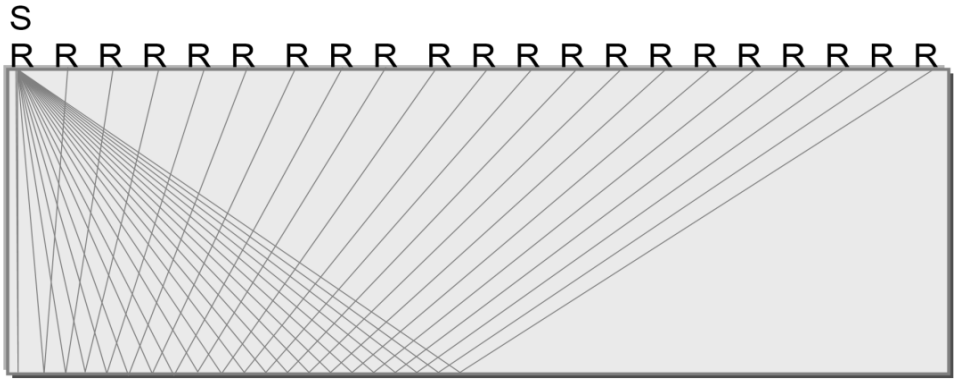

Figure 2.9: The end-on spread acquisition. CDP map. S indicate the source location, R indicate location of receiver (Zhou, 2013).

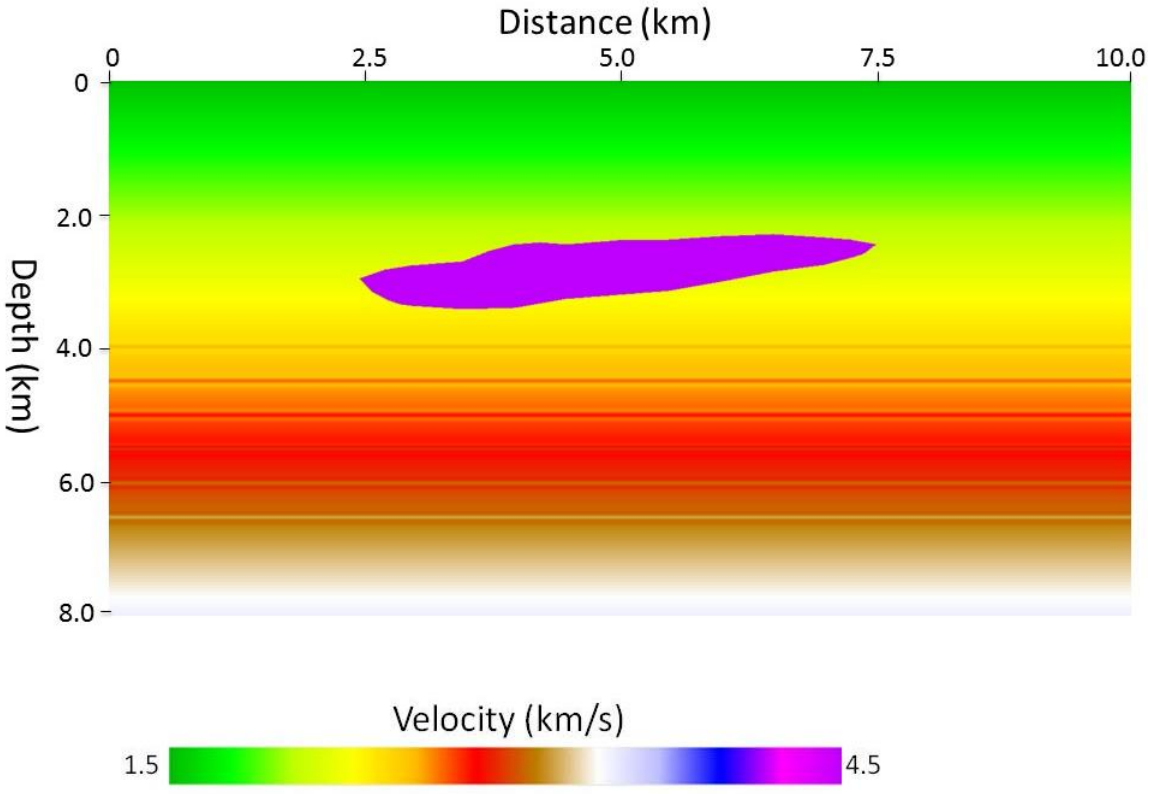

Figure 2.10: True velocity model. It contains 6 horizontal reflectors beneath a salt body (purple).

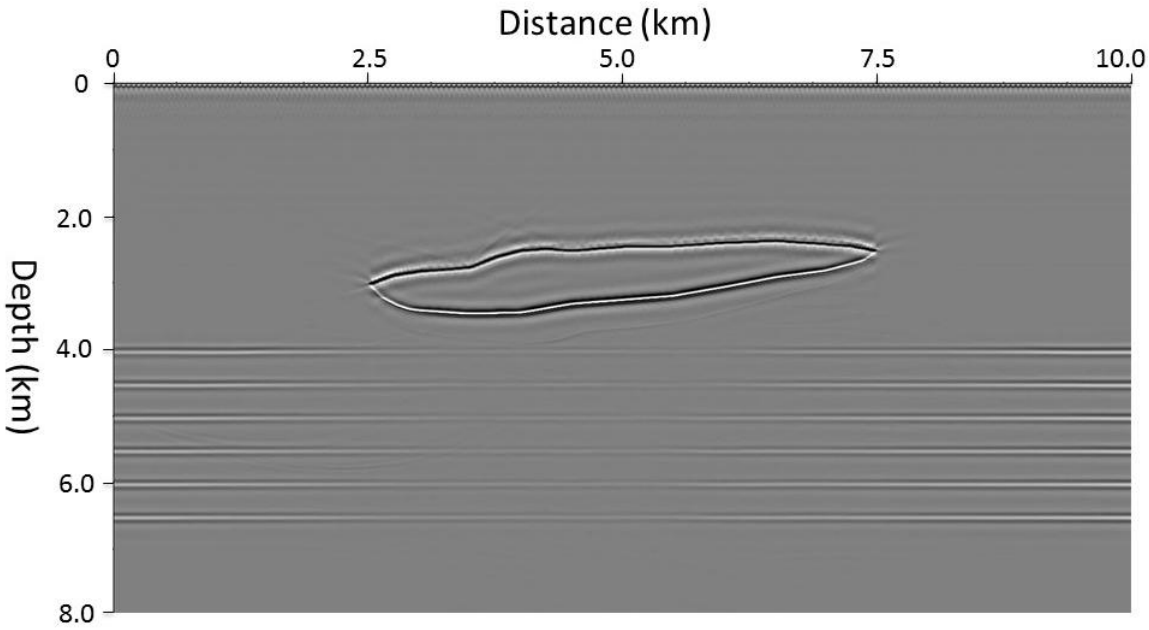

Figure 2.11: RTM image of true velocity model.

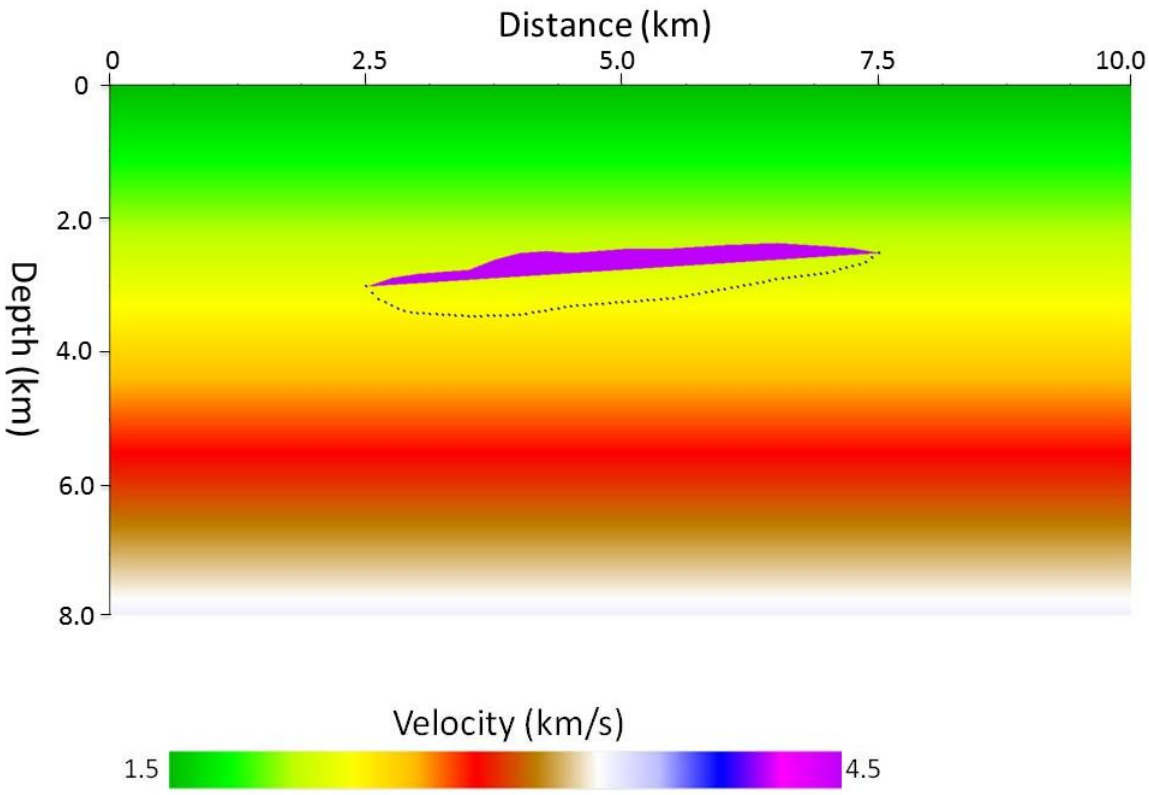

Figure 2.12: An initial velocity model with mispositioned BOS. The dashed line shows the location of true BOS.

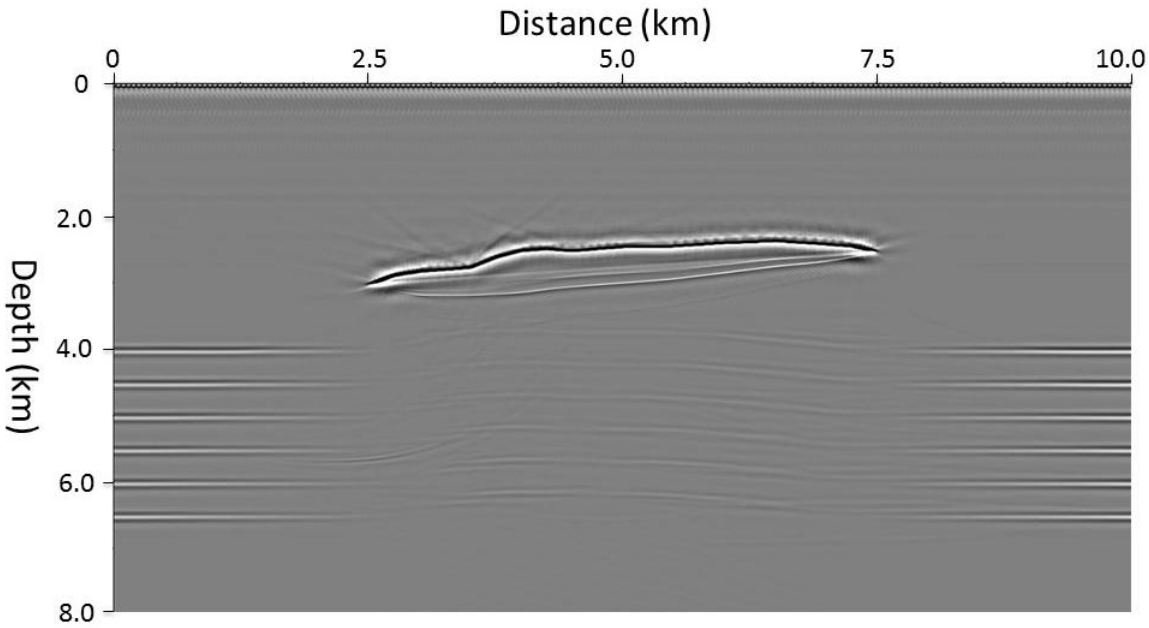

Figure 2.13: RTM image of the initial model.

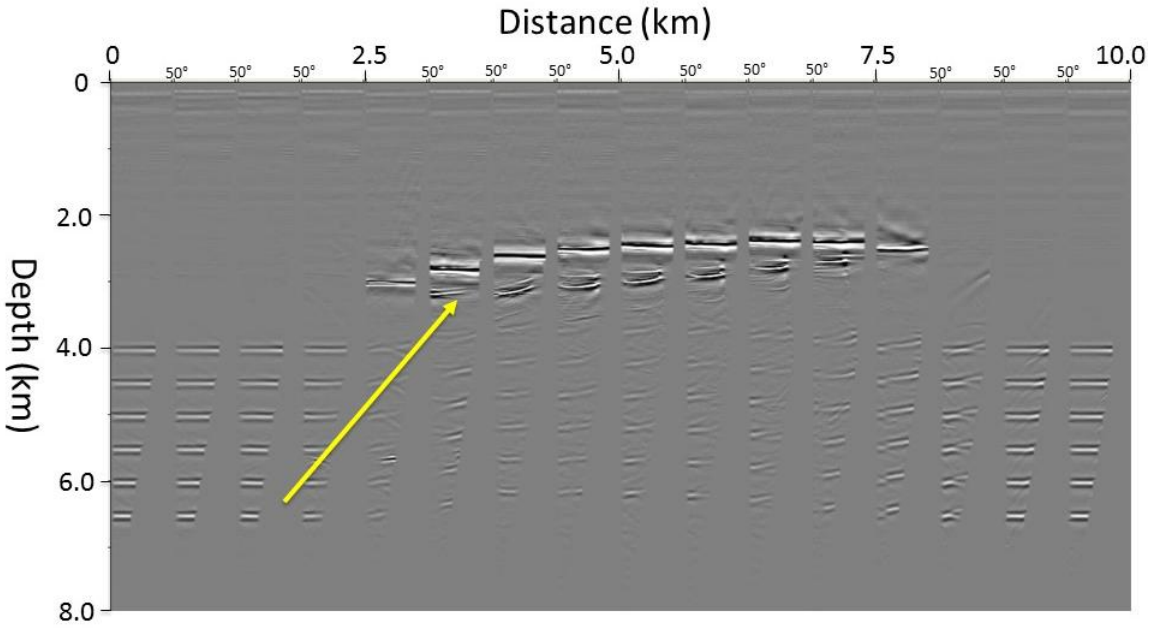

Figure 2.14: ADCIGs from RTM using the initial velocity model. The maximum angle for each gather is 50°. The yellow arrows highlight base of salt at a CDP location.

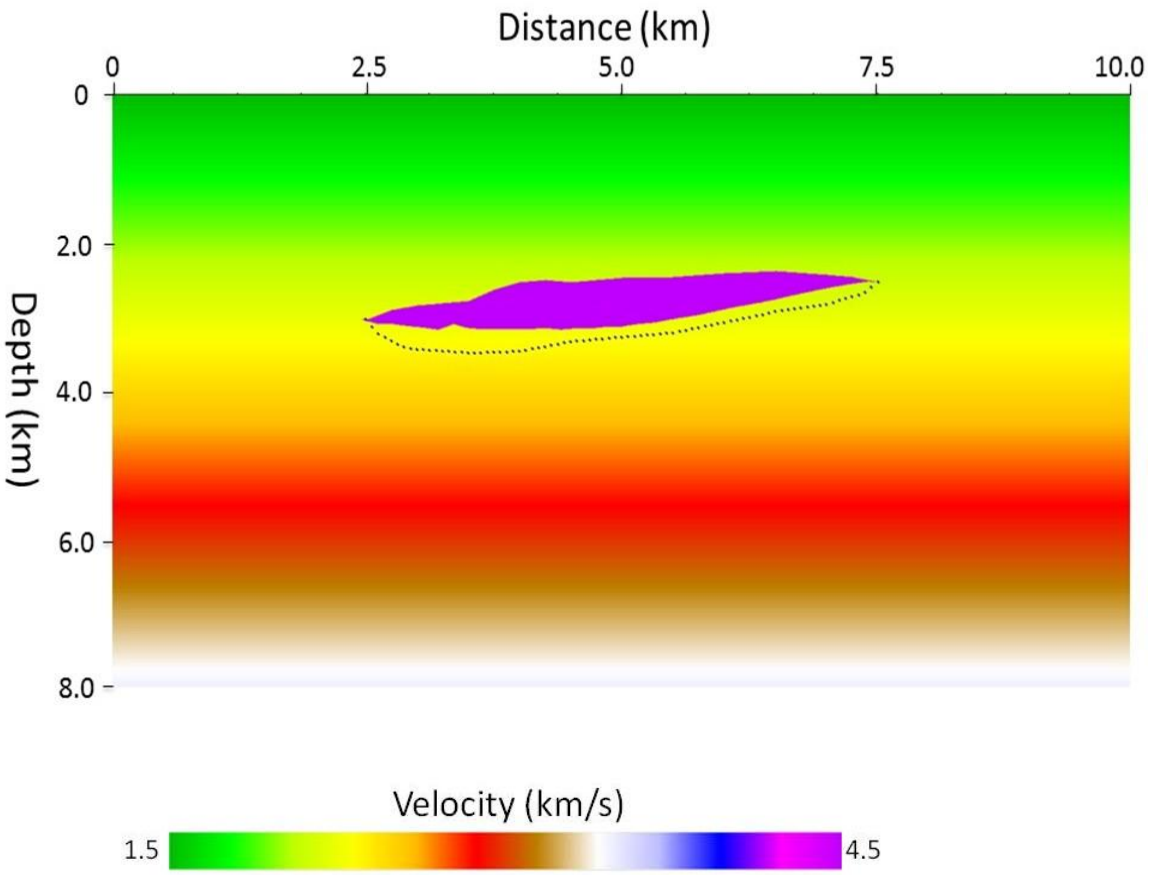

Figure 2.15: First iteration (Tomo1) velocity models based on single-scale RLT. The blue dashed line shows the true BOS location.

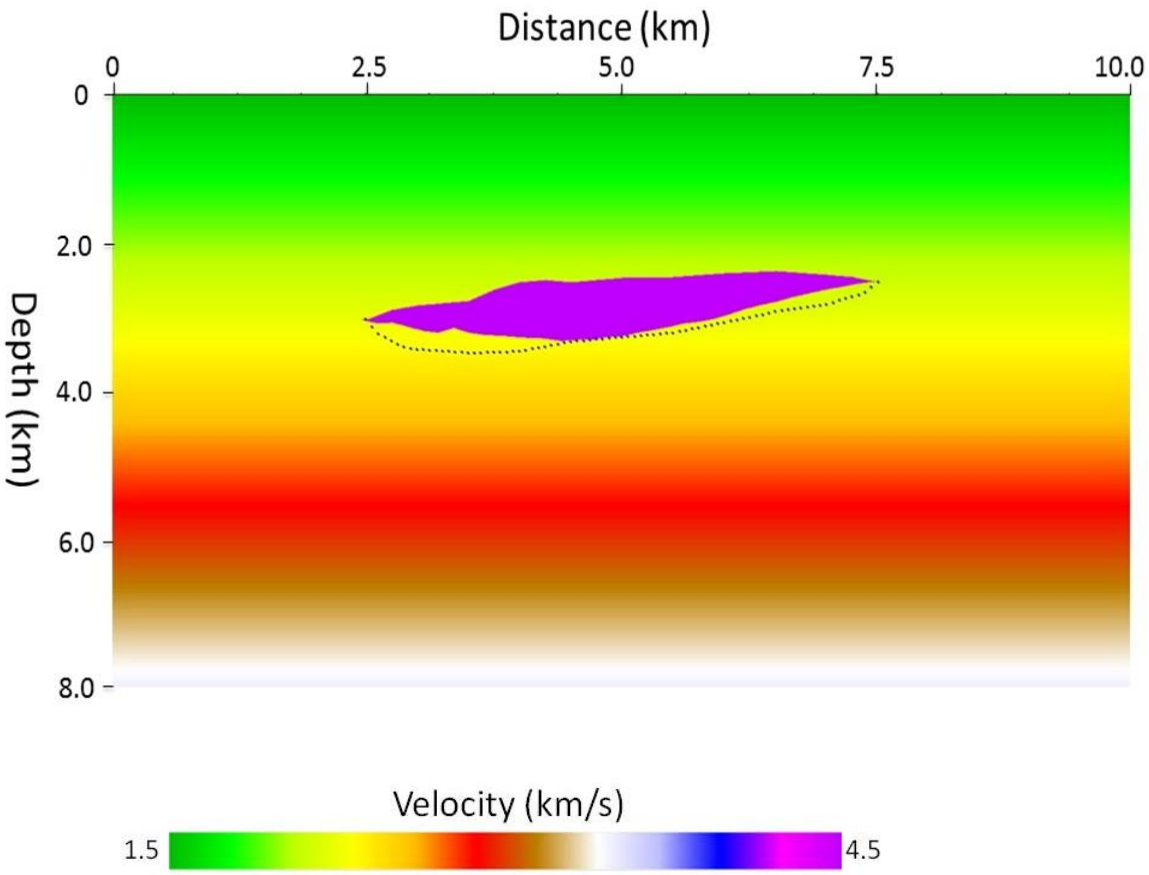

Figure 2.16: Second iteration (Tomo2) velocity models based on single-scale RLT. The blue dashed line shows the true BOS location.

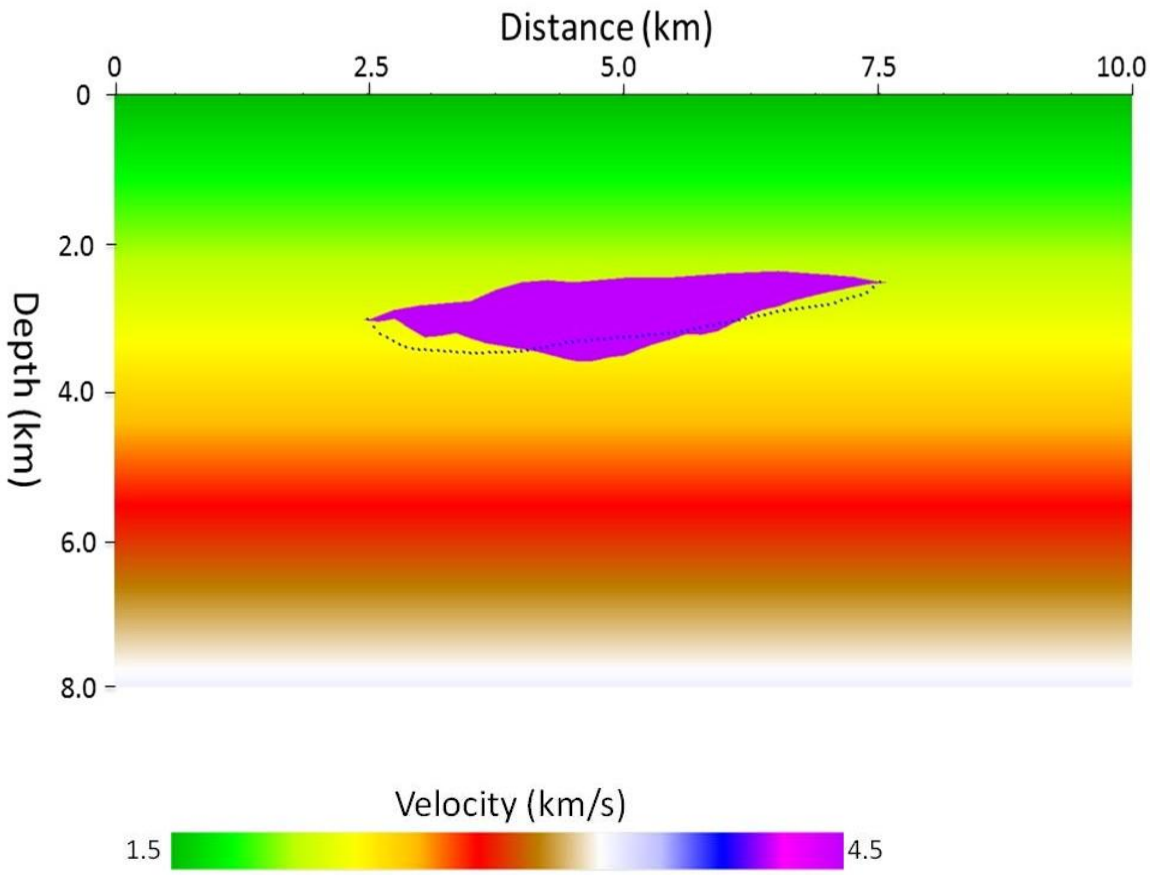

Figure 2.17: Third iteration (Tomo3) velocity models based on single-scale RLT. The blue dashed line shows the true BOS location.

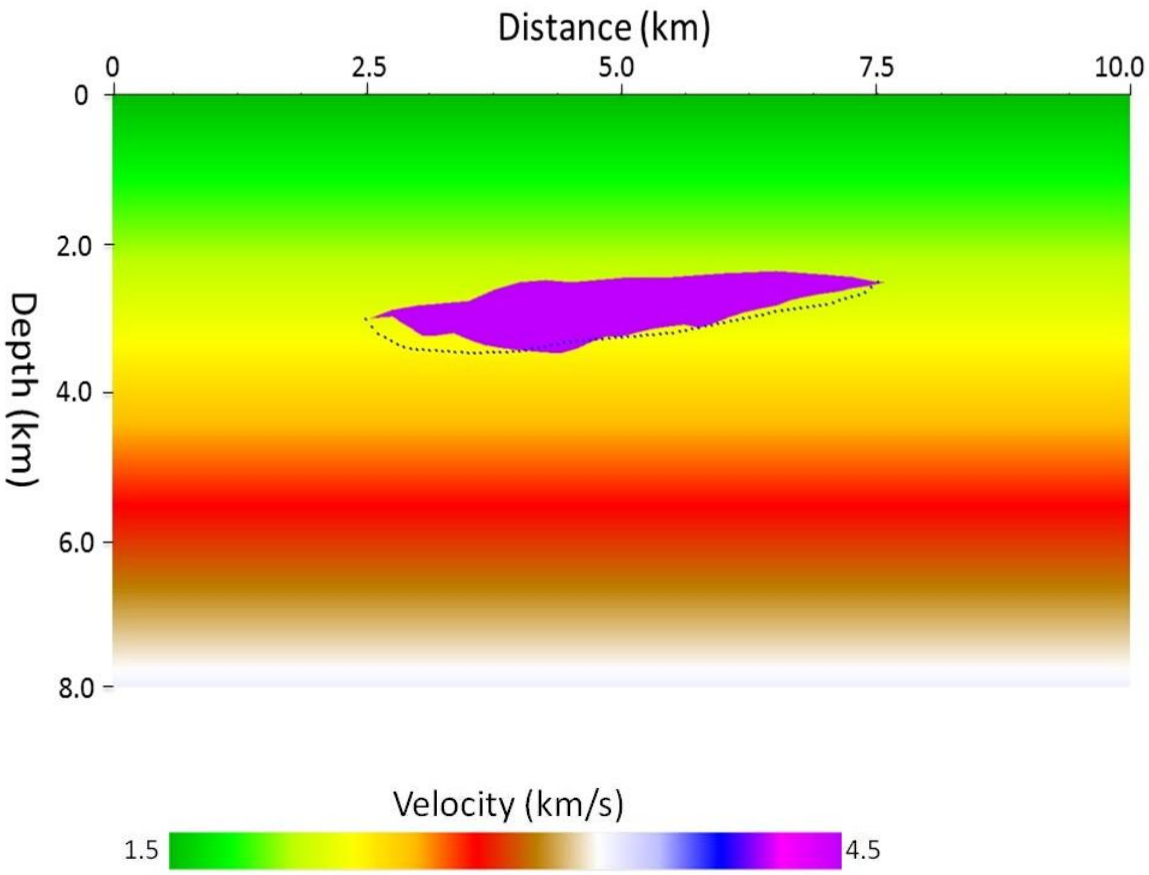

Figure 2.18: Fourth iteration (Tomo4) velocity models based on single-scale RLT. The blue dashed line shows the true BOS location.

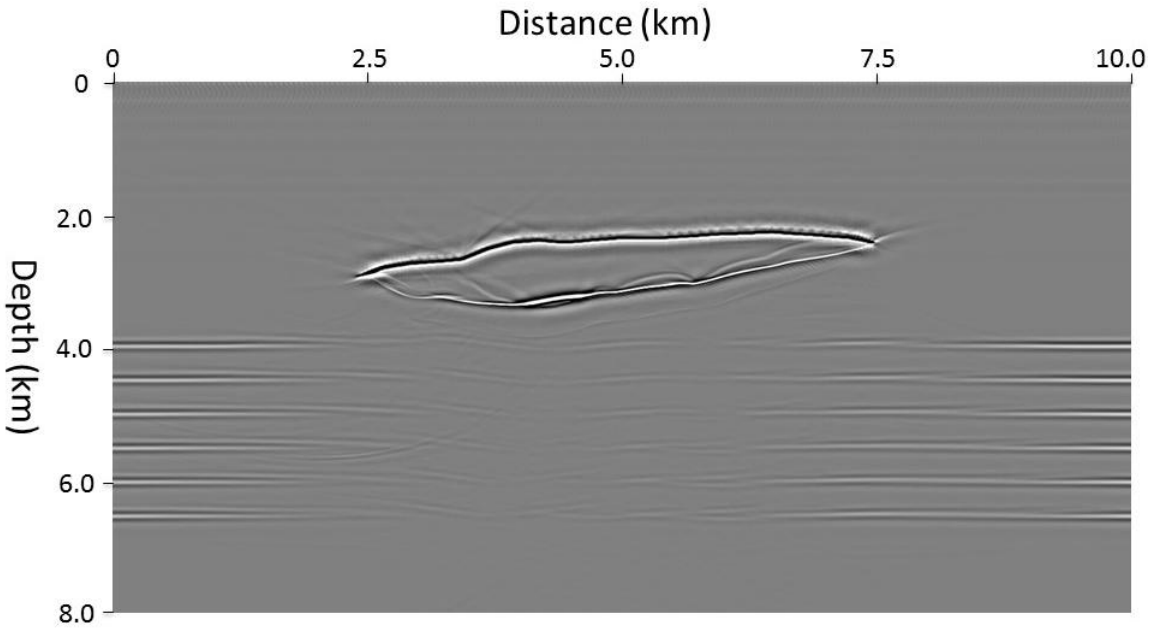

Figure 2.19: RTM image with an updated Tomo4 model from single-scale RLT.

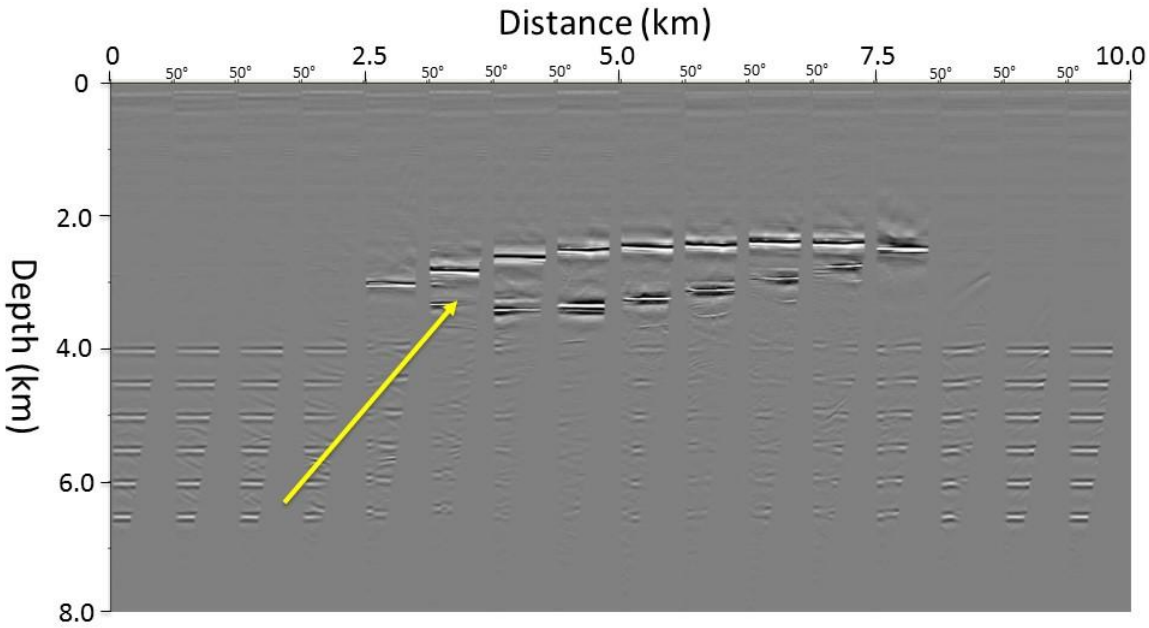

Figure 2.20: ADCIGS of a single-scaleTomo4 model. The arrow highlights the obvious RMOs below the steep dip salt flanks.

2.6 SUMMARY

In this chapter, I have developed RLT to estimate velocity interface geometries. More accurately, it can be called single-scale RLT. This technique has been applied to automatically delineate the BOS as well as to improve the subsalt imaging. Single-scale RLT takes advantage of ADCIGs, thereby eliminating the multi-pathing problem in ODCIGs, which are often used in conventional tomography. The 2D synthetic salt model results showed that this technique can automatically and effectively estimate the geometry of the BOS. As a result, one can construct a more accurate salt model and thereby improve the subsalt image. In this work, we assume that both the overburden velocity and the top-salt geometry are known. These two requirements can be relatively easily realized with standard model building procedures.

However, in geologically complex areas, such as steep dip salt flanks, single-scale RLT still faces challenges in satisfactorily recovering the BOS. Therefore, ADCIGs below the steep dip salt flanks still show significant RMOs. The challenge in recovering the salt flanks is mainly due to uneven ray coverage after ray penetrates through the salt body. I will further resolve this issue in the next chapter.

CHAPTER 3: MULTI-SCALE REFELCTION-LAYER TOMOGRAPHY

3.1 OVERVIEW

Migration tomography is influenced by the grid size of a velocity model. In practice, for a model with a small grid size, traveltime inversion may provide high resolution in areas of good ray coverage area. However, data would be inevitably uneven, and some cells would thus have few or even no rays traversing them. The null space would cause instability and ambiguity in the inversion. Since traveltime tomography depends on ray coverage and cell hit count to constrain the spatial location of velocity anomalies, the uneven distribution of data and ray paths throughout the model may cause smearing artifacts or incorrect velocity features along the ray path. With a larger grid size, more transmitted rays in each grid can improve reliability, but they may sacrifice the resolution.

Different approaches have been developed to overcome this dilemma. The multigrid method is used to accelerate the convergence of a basic iteration from a large grid size to a small grid size. Both waveform tomography and ray tomography have used this to obtain an optimized solution. Since traveltime tomography depends on ray coverage and

cell hit count to constrain the spatial location of velocity anomalies, the uneven distribution of data and ray paths throughout the model may cause smearing artifacts or incorrect velocity features along the ray path. For this reason, the way we handle large spatial variations of ray coverage is to use inversion solutions from multiple scaled tomographic inversion procedure, that is, from the coarsest grid to the finest grid defined in the tomography to seek both long-wavelength features and short-wavelength features. The final model solution is equivalent to the superposition of all inversion solutions with cells on different scales. Multiple-scale tomography (Zhou, 1996) combines short and long wavelengths by superposing a set of sub-models with different cell sizes.

In this chapter, I first describe the method of multi-scale RLT and its implementation. Then, I compare the migration stack and ADCIGs generated from the multi-scale RLT approach using the synthetic data of Chapter 2. Both indicate that inverted velocity distribution of multi-scale RTL has improved. In the end, I conclude that RLT can use a multi-scale strategy to reduce non-uniqueness, and improve inverted velocity distribution. The multi-scale approach has better solutions for updating the velocity model by improving the ray coverage and helping the inversion converge to the global minimum.

3.2 METHOD OF MUTLI-SCALE RLT

Tomography is usually an underdetermined problem, and many different models may yield misfit values within a reasonable tolerance. This non-uniqueness problem in tomographic velocity analysis is largely the result of insufficiency in model parameterization. For a model with small grid size, tomography may provide high resolution in good ray coverage areas; however, the inverted velocity model can be non-unique in poor ray coverage areas. For models with large grid size, more rays transverse in each grid to improve ray coverage and reliability, but the resolution may be sacrificed. Traditional single-scale tomography may produce under-determinacy at places of insufficient ray coverage. On the contrary, a multi-scale tomography scheme can cope with uneven ray coverage to balance the long- and short-wavelength components of the solution model (Zhou 1996, 2003).

In single-scale RLT, the interface was parameterized as a set of control points, however, given the limited number of rays, some of the control points may not be covered by the rays (Figure 3.1). The consequence of this uneven ray coverage is that the inversion result for these control points is not reliable. This explains why for the steep dip salt flank area, our single-scale RLT result is not very satisfactory. In multi-scale RLT, we decompose the model as a linear combination of different scales (Figure 3.2). For the scale with long wavelength components, the ray converge for the entire model space

becomes more even. And as a result, the inversion result will become more stable and reliable than the scale with short wavelength components.

The MST scheme decomposes the solution perturbation at any location into components of various spatial resolutions called sub-models and simultaneously inverts for solutions of all sub-models. The final solution is to superpose all the sub-model solutions and the MST model, which is smoother and geologically more plausible than the SST model. In this paper, we extend the MST method to determine the interface geometry using reflection rays. Similar to equation 2.7, we can build the linear system for multi-scale RLT as follows

$$\sum_{n}^{N} w_n \mathbf{A}_n \Delta \mathbf{h}_n = \Delta \mathbf{t} \tag{3.1}$$

where n is the scale index and N is the total number of scales (sub-models) for inversion. Here, w_n is the scaling coefficient for each sub-model, and the sum of all w_n must be 1. In our example, we simply set $w_n = 1/N$. The number of unknowns in the n+1 scale is twice that of the scale n. The misfit function is more linear to the long wavelength component of the model than to the short wavelength. By reducing nonlinearity, multi-scale RLT is able to mitigate the local minima problem commonly encountered in tomography.

The implementation of multi-scale RLT is similar to the singe-scale approach described in Chapter 2. RMOs extracted from pre-stacked migrated gathers are used to update the velocity interface model. However, the model of multi-scale RLT is composed

into a linear combination of different sub-models. Each sub-model has a different number of control points and is set up in equation 3.1 for matrix inversion. All sub-models are then converted to the finest grid, and values at the same location are summed to obtain the final model update.

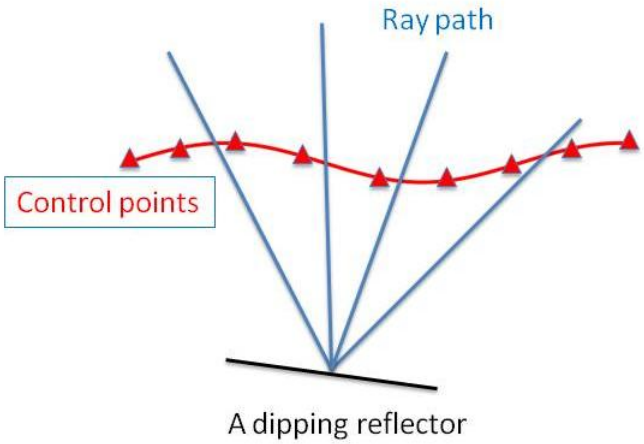

Figure 3.1: Ray distribution for single-scale tomography. Blue lines indicate the ray path, red line is the interface. Red triangles show the locations of control points.

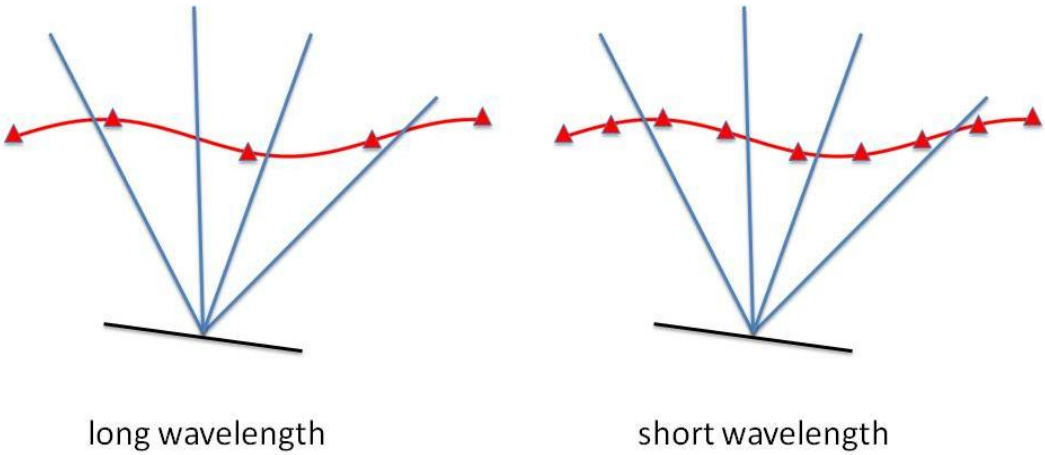

Figure 3.2: Ray distribution of two different scales for multi-scale tomography. The scale with long wavelength components (left), the ray converge for the entire model space become more even. The model with short wavelength scale (right) has uneven the ray converge.

3.3 SYNTHETIC EXMAPLE

For fair comparison, the same synthetic dataset and initial model of single-scale RLT were used to test multi-scale approach. Exactly four iterations were performed to update the BOS model. The main cause of the low quality of the inverted image is uneven ray coverage. To mitigate the depth image artifacts, multi-scale RLT is introduced to the workflow of migration velocity analysis.

Multi-scale RLT starts from the same initial model (Figure 2.12) as the single-scale RLT. As described in Equation 3.1, the number of control points on the BOS of sub-models is different when representing different wavelengths of the spatial variations of the BOS. Four sub-models are used in the inversion for multi-scale RLT. The first sub-model has 41 control points to represent the depth variables of the interface; the second sub-model omits every other original control point and results in 21 variables. Likewise, the third and the fourth sub-models have 11 and 5 variables, respectively. Therefore, a total of 83 (41 + 21 + 11 + 5) variables are used in the multi-scale RLT to depict the BOS. During each iteration, the interface perturbations of four sub-models are converted to the finest grid for superposition to obtain an updated velocity interface.

Figure 3.3 gives the interface velocity based on the superposition of four sub-models after the first iteration. In comparison with single-scale Tomo1 (Figure 2.15), a

multi-scale solution yields better results, such as steep dip salt flanks. Figure 3.4, Figure 3.5, and Figure 3.6 indicate the velocity model update to the fourth iteration model.

With the same input, multi-scale RLT yields superior solutions compared to the single-scale RLT, and it matched very well with the true model (Figure 2.10). The BOS geometry produced after four iterations of multi-scale RLT (Figure 3.6) was generally smoother and geologically more plausible than the single-scale RLT (Figure 2.18). The artifacts of multi-scale RLT have mostly been eliminated, especially in the steep dip salt flank areas.

Compared to ADCIGs of single-scale RLT (Figure 3.8), the ADCIGs of multi-scale RLT shown in Figure 3.9 present more coherent and flatter events, especially in the steep dip area as pointed out by the arrow and circles. The multi-scale approach has greatly reduced the residual move out that dominates the initial ADCIGs.

Sub-salt horizons of the RTM image with the multi-scale model (Figure 3.7) are also better focused and more continuous than the single-scale RLT result (Figure 2.19). The multi-scale RLT result is smoother and geologically more plausible than the single-scale RLT model.

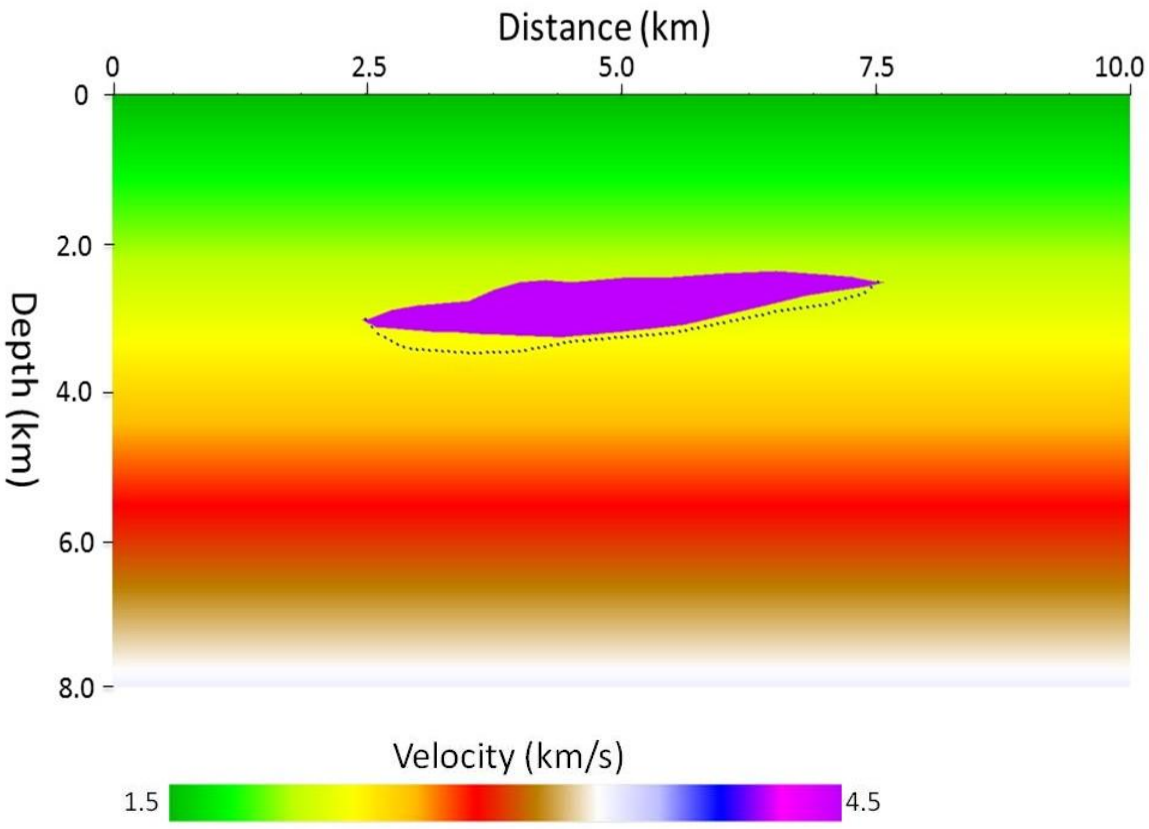

Figure 3.3: First iteration (Tomo1) velocity models based on multi-scale RLT. The blue dashed lines show the true BOS location.

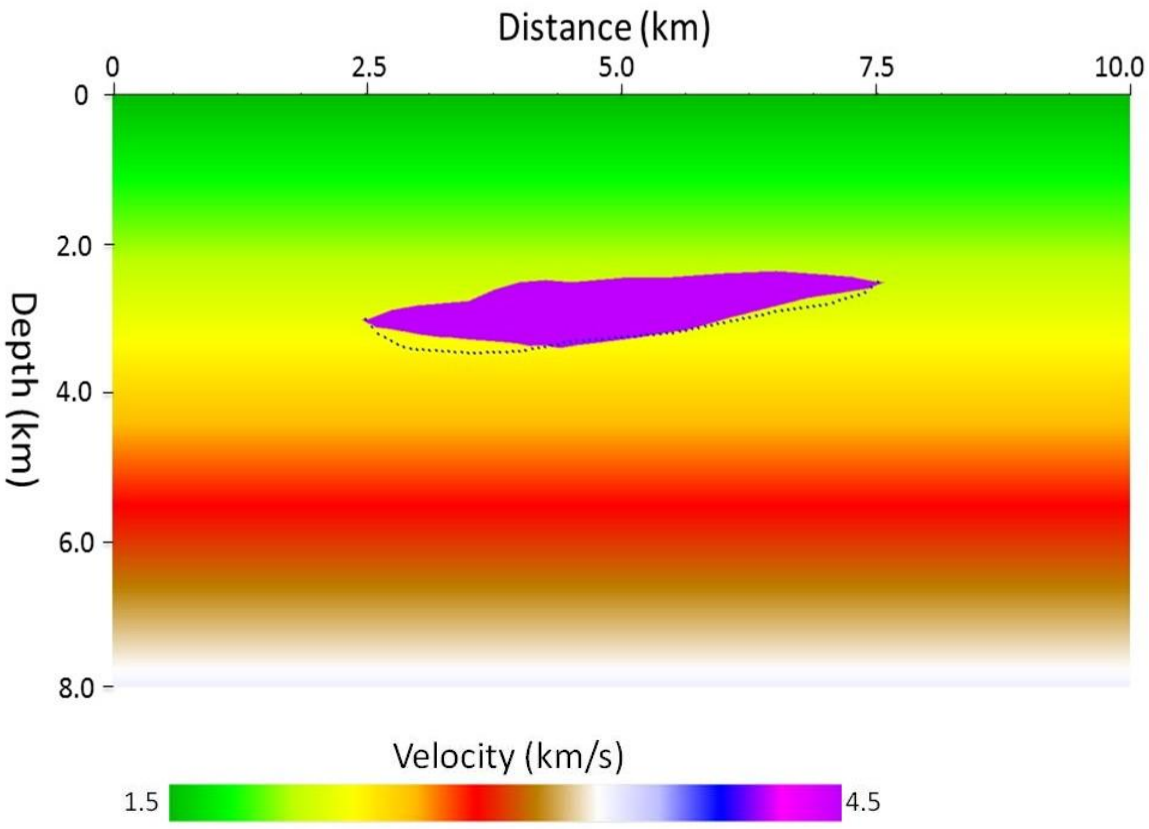

Figure 3.4: Second iteration (Tomo2) velocity models based on multi-scale RLT. The blue dashed lines show the true salt base location.

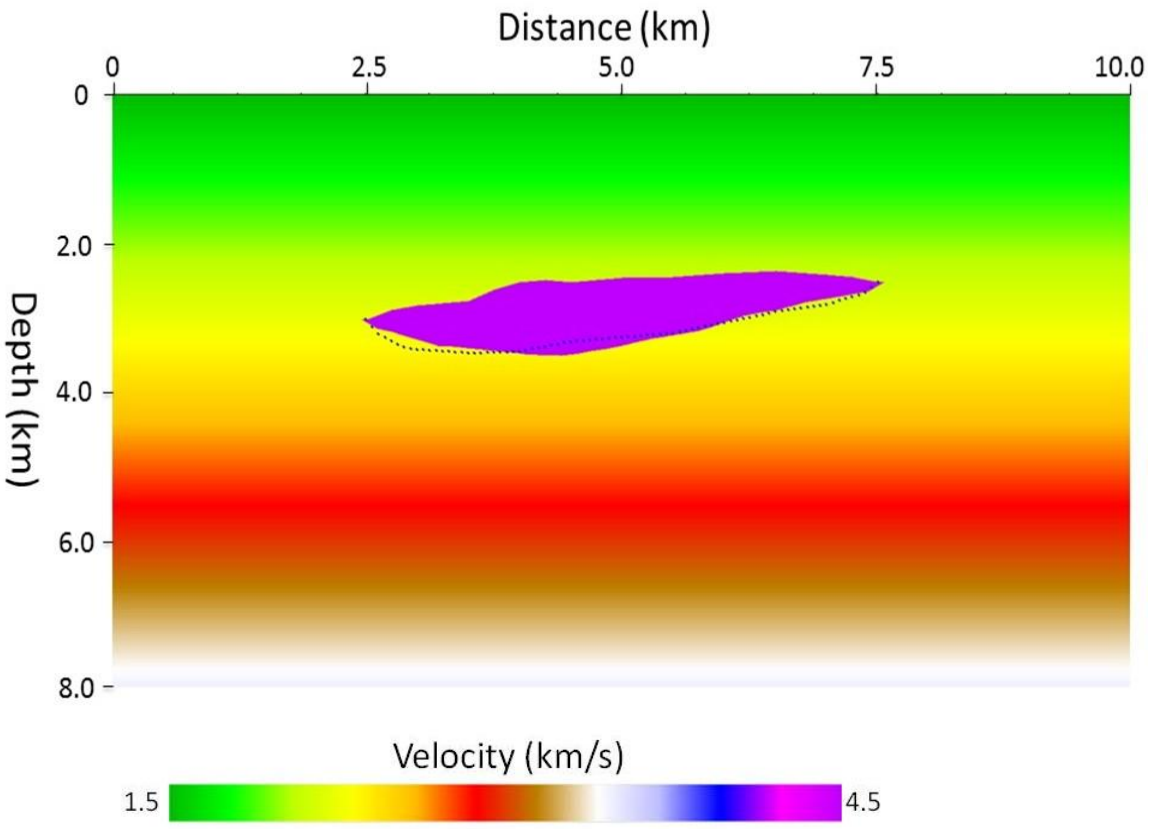

Figure 3.5: Third iteration (Tomo3) velocity models based on multi-scale RLT. The blue dashed lines show the true BOS location.

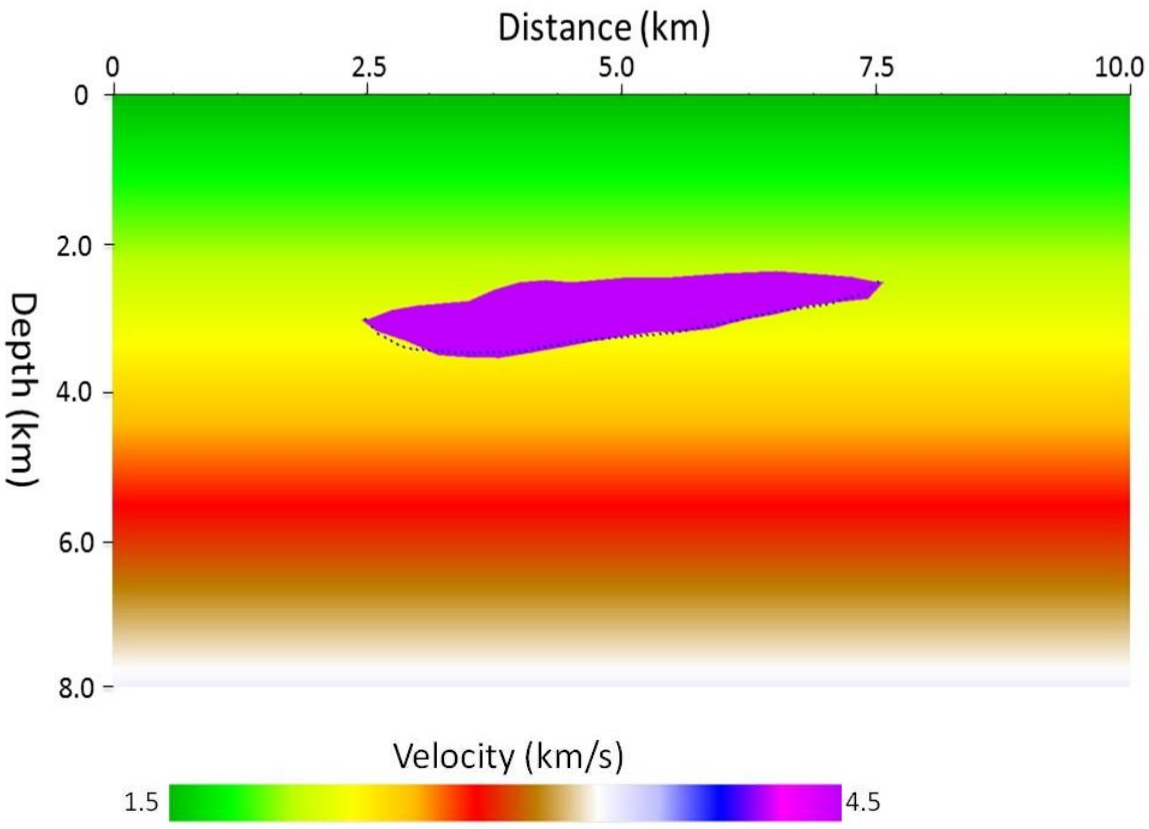

Figure 3.6: Fourth iteration (Tomo4) velocity models based on multi--scale RLT. The blue dashed lines show the true BOS location.

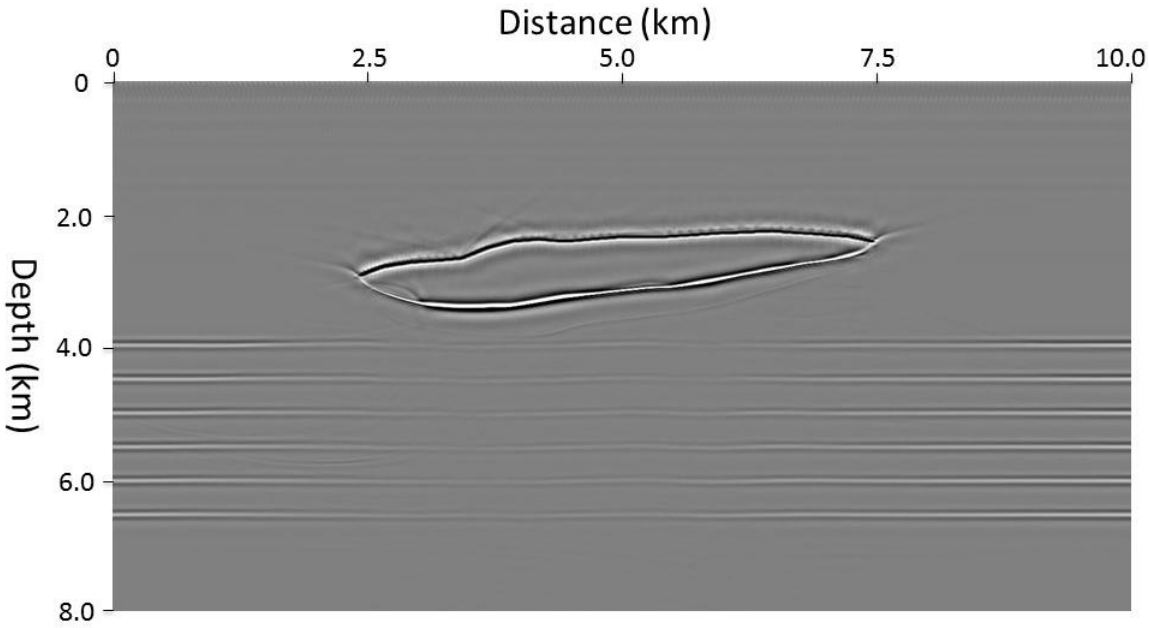

Figure 3.7: RTM image of the multi-scale RLT Tomo4 model.

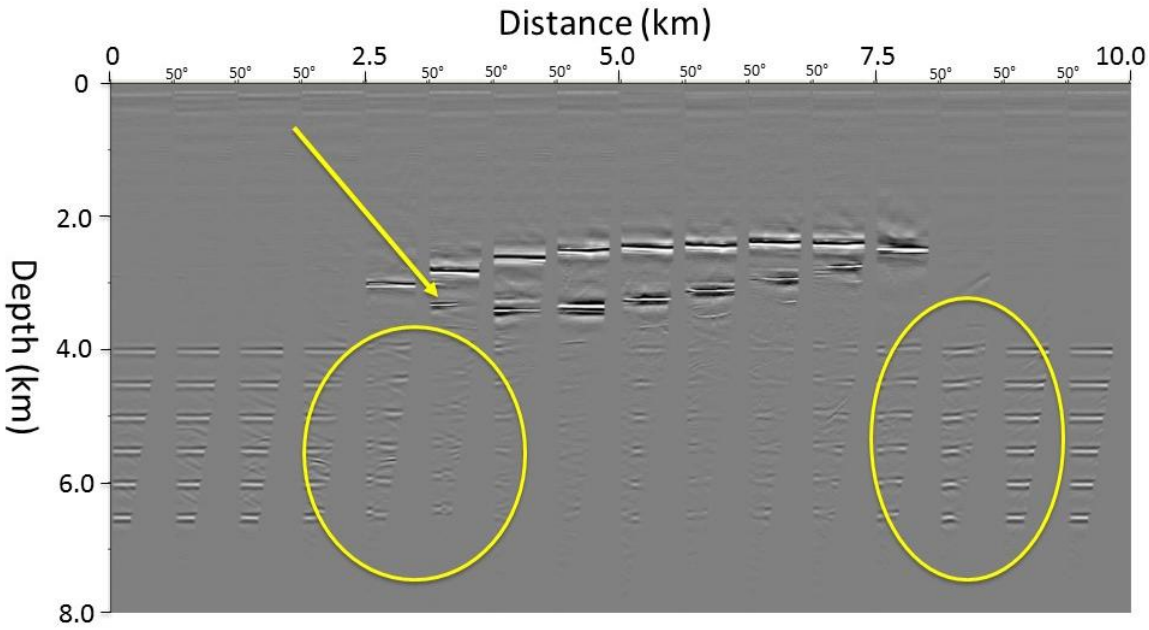

Figure 3.8: ADCIGS with the single-scale RLT tomo4 model. The maximum angle for each gather is 50°. The yellow arrow and circles highlight the flatness of the BOS and the sub-salt reflectors.

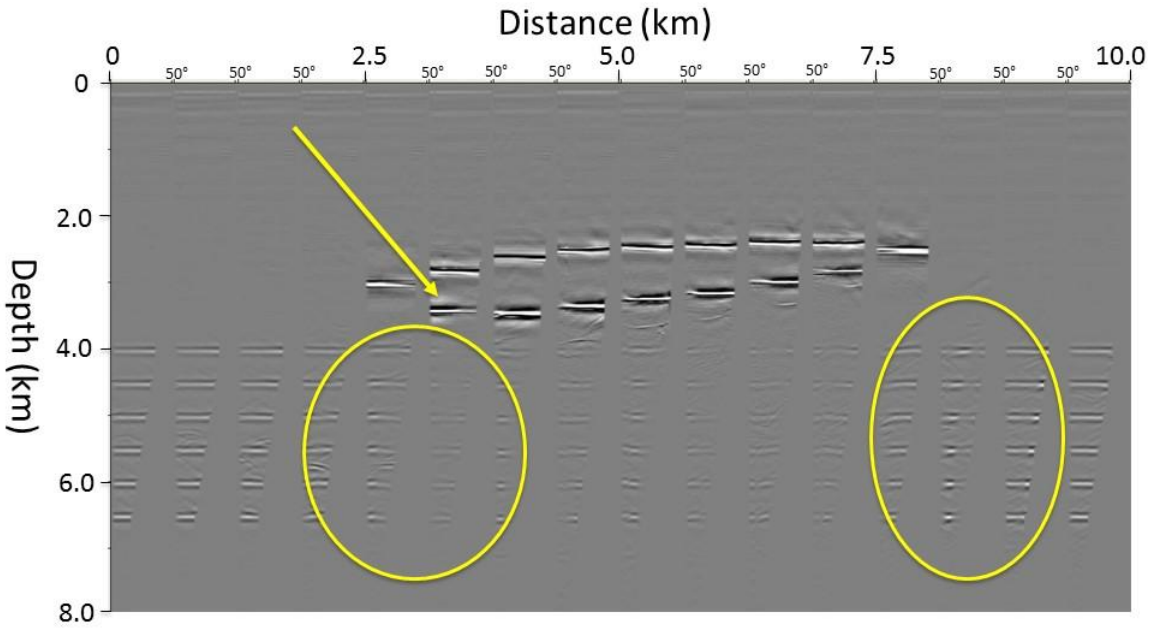

Figure 3.9: ADCIGS with the multi-scale RLT tomo4 model. The maximum angle for each gather is 50°. The yellow arrow and circles highlight the flatness of the BOS and the sub-salt reflectors.

3.4 SUMMARY

Both the single-scale in Chapter 2 and multi-scale approach in Chapter 3 demonstrated the ability of RLT to resolve salt model changes. Compared with single-scale approach, the artifacts of multi-scale RLT have mostly been eliminated. The bottom two figures show the corresponding CIGs. RLT has greatly reduced the residual move out that dominates the initial CIGs. The solution error chart (Figure 3.10) indicates the two scales in which tomography can successfully reduce errors during inversion. Using the multi-scale strategy, RLT can reduce non-uniqueness. Compared with single-scale RLT, multi-scale RLT provides better solutions for updating the velocity model. Both the migrated stacks and the common image gathers indicate that the inverted velocity distribution of multi-scale RTL has improved.

In summary, multi-scale RLT improves the ray coverage and helps the inversion converge to the global minimum in velocity model building. The synthetic example indicates that multi-scale RLT can better constrain the layer interfaces and handle complex media for which the single-scale approach lacks efficiency in updating velocity. Although both multi-scale and single-scale RLT converge with iterations, multi-scale RLT provided more accurate velocity and efficiency than the single-scale approach. The 2D synthetic test shows good probability for inverting the interface geometer using RLT. In the next chapter, this velocity analysis algorithm is extended to the 3D case.

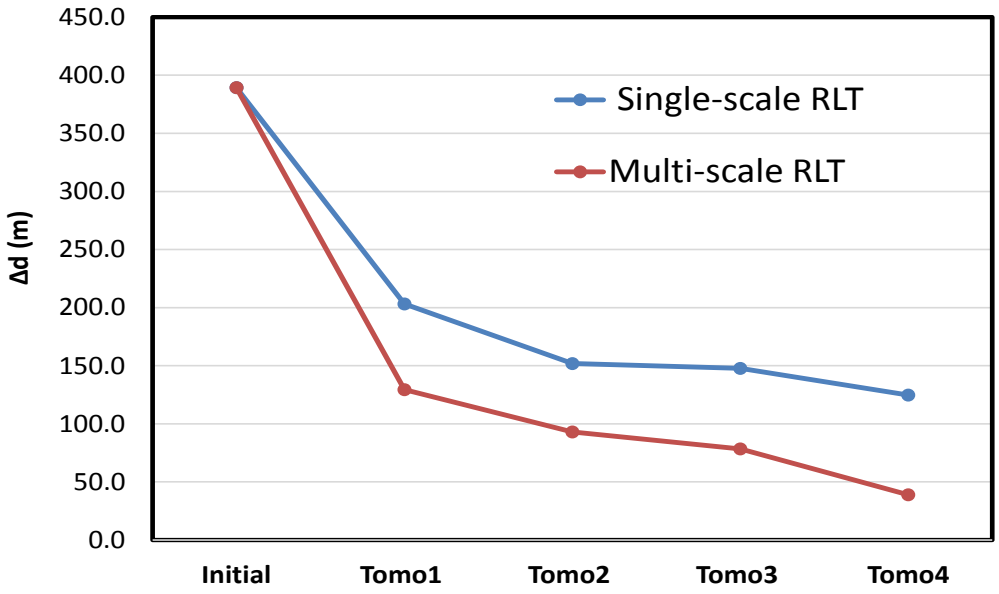

Figure 3.10: Model misfit versus iterations for single-scale RLT and multi-scale RLT. Δd is the standard deviation of the depth difference between updated BOS and the true BOS.

CHAPTER 4: 3D REFLECTION-LAYER TOMOGRAPHY

4.1 OVERVIEW

Three-dimensional (3D) seismic technology has extensively advanced since the 1980s. A typical problem with two-dimensional (2D) seismic data processing and imaging is that there are always some reflected seismograms originating from the out-of-plane reflectors, which 2D migration cannot handle properly. A 3D seismic survey provides the additional information to permit full 3D migration in multiple azimuth directions, and it has evolved from narrow azimuth (NAZ) to wide azimuth (WAZ), and even to full azimuth (FAZ). The evolution of the 3D seismic survey has substantially improved the signal-to-noise ratio in acquired data and as a consequence, has improved the image quality. 3D seismic data have had a substantial impact on the successful exploration and production of hydrocarbons (Richard *et al.*, 2004).

Since 3D surveys are being increasingly adopted to achieve a higher degree of spatial resolution and to obtain a more trustworthy image of the subsurface geology than 2D surveys, it is important to extend RLT from 2D to 3D for more practical applications. In this chapter, I first introduce the model parameterization and algorithm of 3D RTL. Then, a 3D synthetic test is designed to demonstrate 3D RLT. The results show that the migrated image and ADCIGs can be significantly improved using this approach.

4.2 METHOD OF 3D RLT

In 3D RLT, the model parameterization (Figure. 4.1c), similar to the as 2D approach, is composed of a gridded velocity model (Figure.4.1a) and a layered interface model (Figure.4.1b). The layer interfaces are deformable by adjusting the vertical positions of the corner nodes (control points). During inversion, the variables only update at control points to effects the interface model. Each control point has the fixed x and y values on the surface but adjustable depth. During 3D RLT inversion, the updated layered interface model is converted to the gridded velocity model for subsequent migration and modeling.

Like the 2D approach, 3D RLT updates the velocity interfaces by minimizing RMO in the migrated CAGs. Thus, the connection between RMO and the interface model also uses equation 2.4. However, the ray intersects with a velocity interface in the 3D case, which is more complex than 2D RLT.

Figure 2.7 depicts a ray intersecting with a velocity interface in 3D. In interface model parameterization, each interface control point provides velocity information below and above the interface,

$$\frac{\partial t_k}{\partial d_{i,j}} = \left(\frac{1}{V_{i,j}^{below}}\cos\alpha - \frac{1}{V_{i,j}^{above}}\cos\beta\right) \bullet w_{i,j}\,, \quad (4.1)$$

Where ray propagating angles α and β above and below the interface obey Snell's law and, $V_{i,j}^{below}$ and $V_{i,j}^{above}$ are velocities below and above the interface at the *(i, j)th* grid, respectively. $w_{i,j}$ is the weighting term of *(i, j)th* grid.

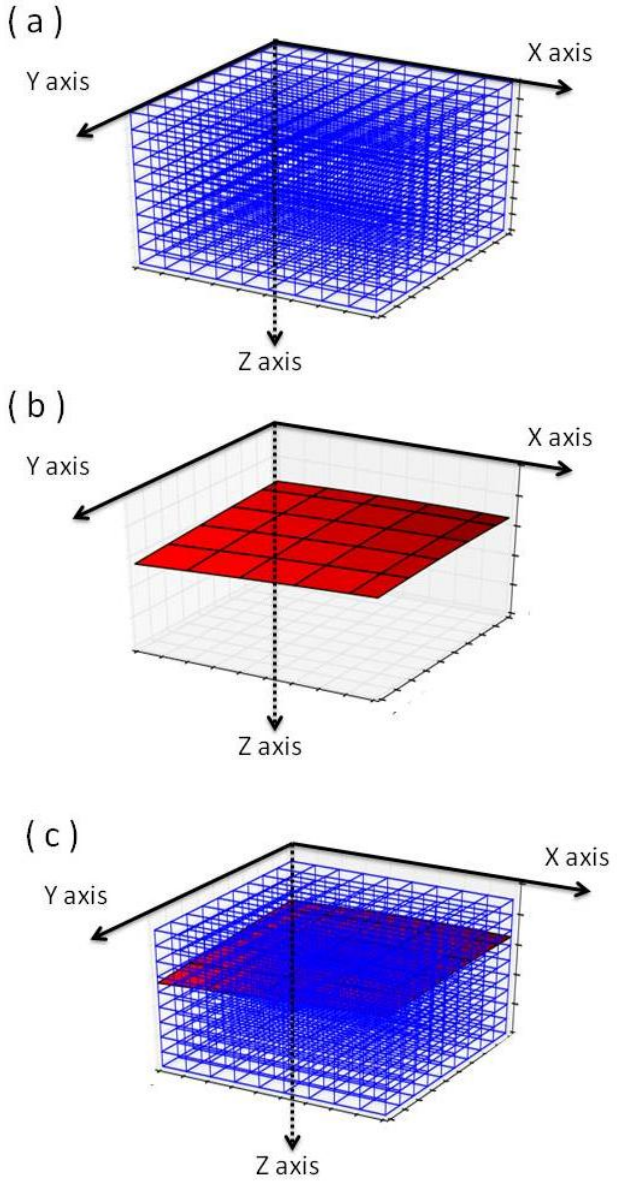

Figure 4.1: (a) A gridded velocity model. Each blue cube has its own velocity. (b) A layered interface model. Red surface are velocity interfaces. (c) RLT model in 3D case.

Figure 4.2 shows a seismic ray inside one cell, where the weight term can be obtained by Lagrange interpolation of the parameter perturbation at intersection point x:

$$w_{i,j} = \prod_{m=0,n=0}^{1} \frac{\left\| x - x_{i+n,j+m} \right\|}{\left\| x_{i,j} - x_{i+n,j+m} \right\|}$$

where, $\|....\|$ stands for the distance between two points.

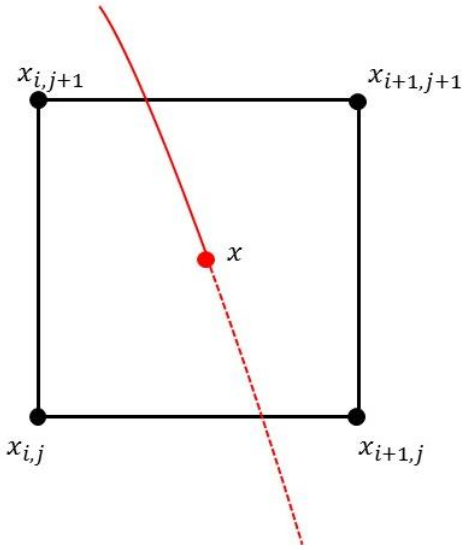

Figure 4.2: Schematic illustration of a ray going through one interface. *x* (red point) is the intersection point. $x_{i,j}$, $x_{i+1,j}$, $x_{i,j+1}$ and $x_{i+1,j+1}$ (black points) present the control points surround *x*.

4.3 SYNTHETIC EXAMPLE

A 3D synthetic test is designed to demonstrate the validity of this approach. The true velocity model (Figure 4.3) contains a salt body with a velocity 14,500 ft/s embedded in a 1D gradient background velocity ranging from 7 kft/s to 13kft/s. Three horizons beneath the salt provide reflection signals for the inversion. A typical survey geometry is designed

to generate synthetic common shot gathers with 15Hz finite difference forward modeling, which is different from the RTM engine. The CDP interval of inline and cross-line is 55ft, and the depth resolution of the velocity model is 30ft.

With this true model, a migrated image (Figure 4.4) shows the superb focus and continuity of both the salt boundary and the sub-salt reflectors, and it locates these events at the right positions.

The BOS of the initial model (Figure 4.6) is significantly deviated from the true geometry, which is indicated by the dashed curve. The RTM image (Figure 4.7) with the initial velocity model shows severe defocus and discontinuity below the salt, indicating the artifacts in the velocity destruction and incorrect salt structure. ADCIGs correspond to the migrated stack in Figure 4.14 by showing the curved events in the defocused subsalt areas. The maximum angles of each gather are 40°, with an increment of 2°. The subsalt reflectors in the initial RTM ADCIGs present significant RMOs, which can be used to improve the BOS.

Starting from the initial model, the BOS of the first iteration (Figure 4.9) moves toward the right direction; the second iteration (Figure 4.10) continues to improve the BOS; the BOS of the third iteration (Figure 4.11) starts to be over-corrected at boundary of salt flank; the fourth iteration (Figure 4.12) tries to bring some of the over-corrected BOS back towards the right direction. Compared to the true model, a 3D RLT solution of the

fourth iteration already shows a reasonable result and the general BOS boundary features are recovered. The migrated stack image of the fourth iteration model (Figure 4.13) is focused and continuous. Compared with the gathers of the initial model (Figure 4.14), most reflection events of the fourth iterations (Figure 4.15) become flatter in both the base of salt and subsalt.

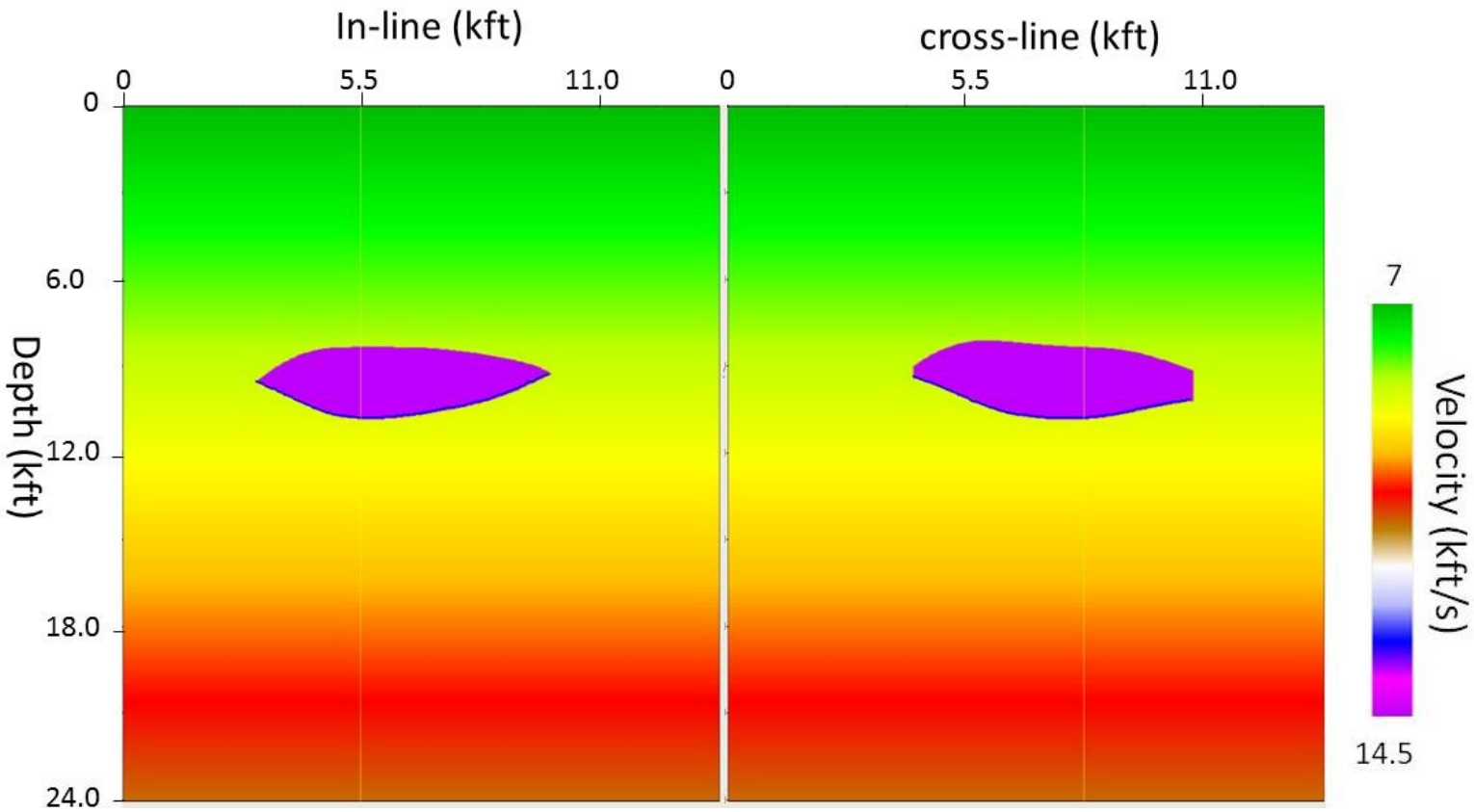

Figure 4.3: 3D true velocity model at in-line (left) and cross-line (right).Salt body (purple) is imbedded in 1D background sediment velocity. The blue lines show true BOS location

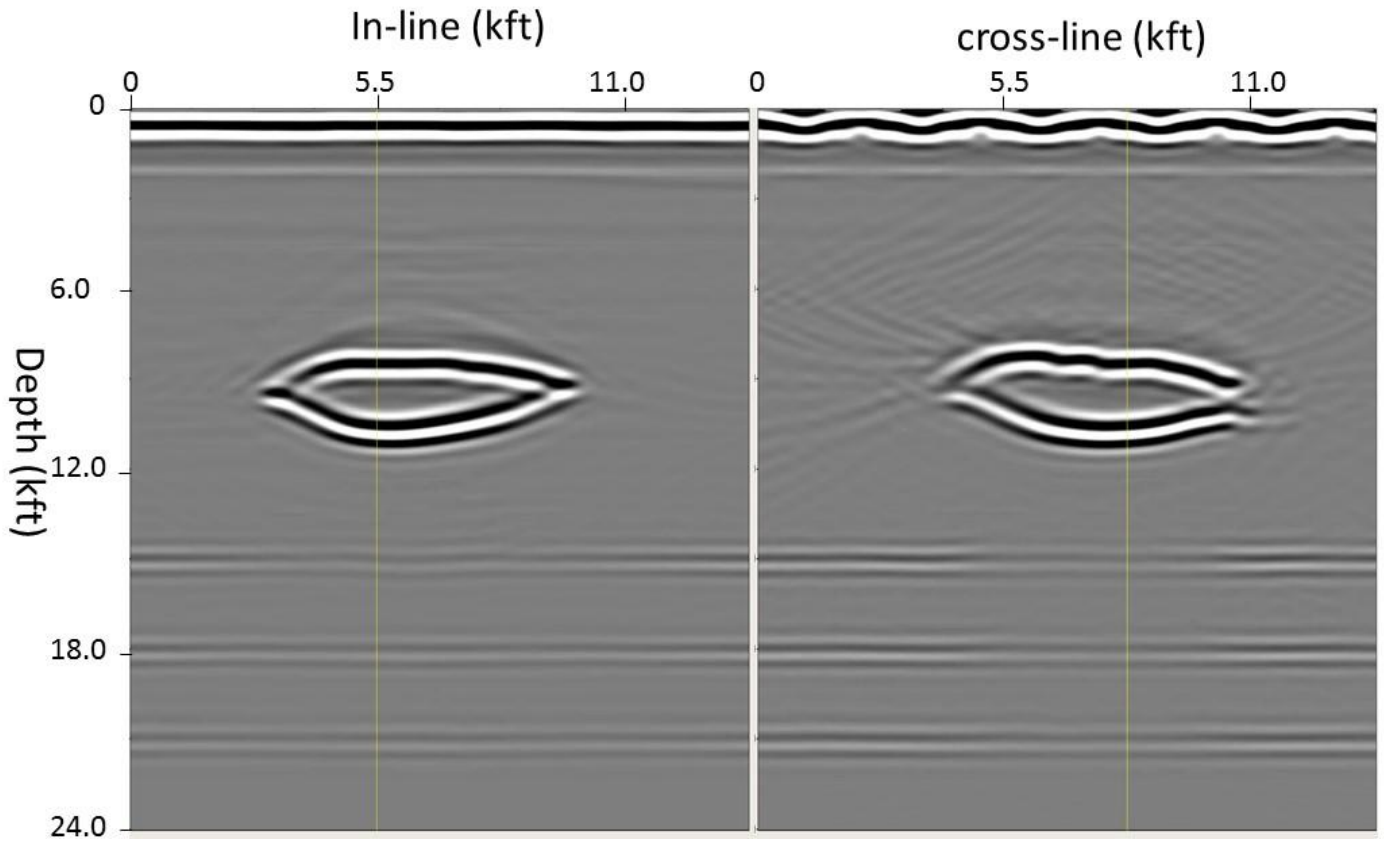

Figure 4.4: 3D RTM image of in-line (left) and cross-line (right) using true velocity model (Figure 4.5:).

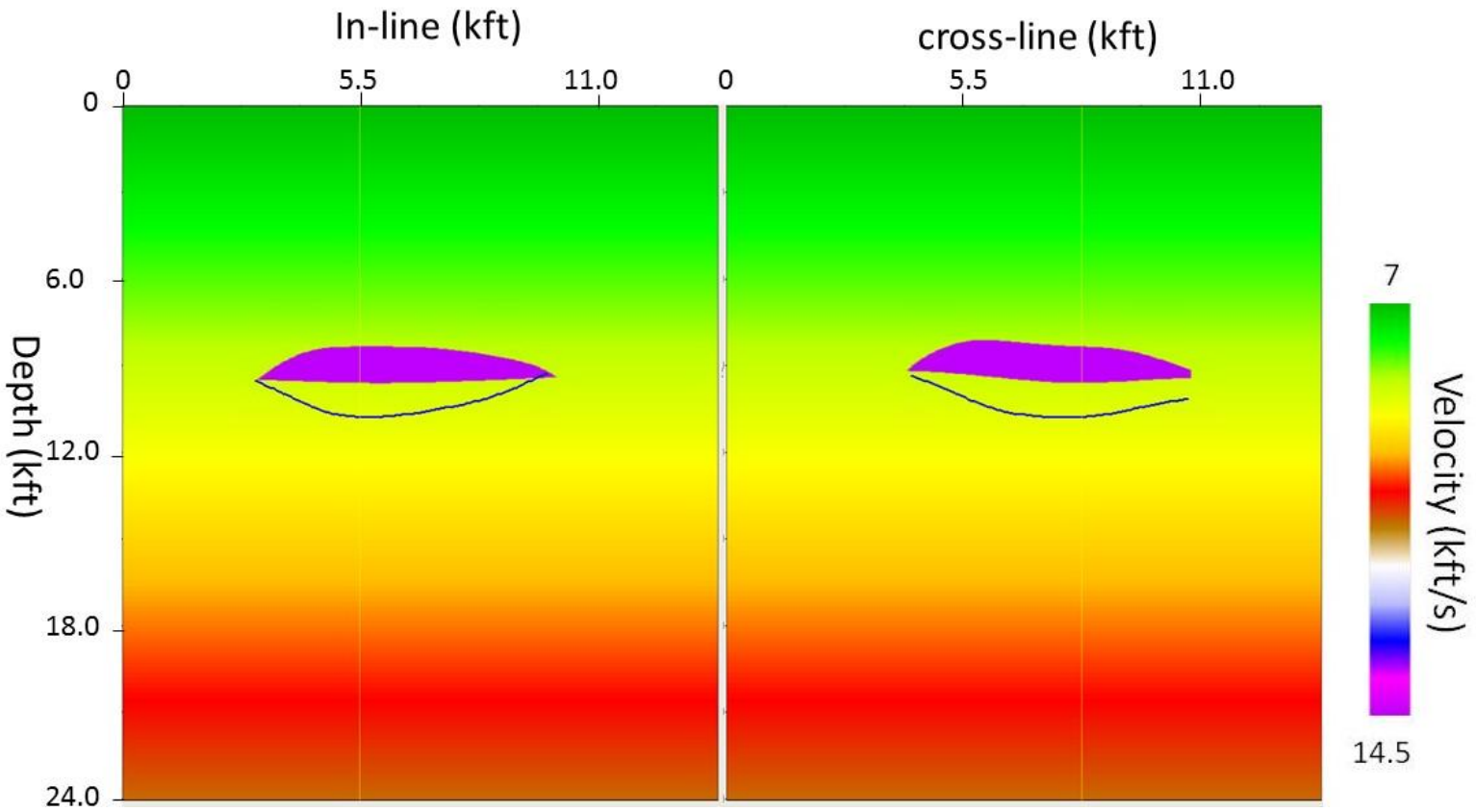

Figure 4.6: 3D initial velocity model at in-line (left) and cross-line (right). The blue lines show true BOS location.

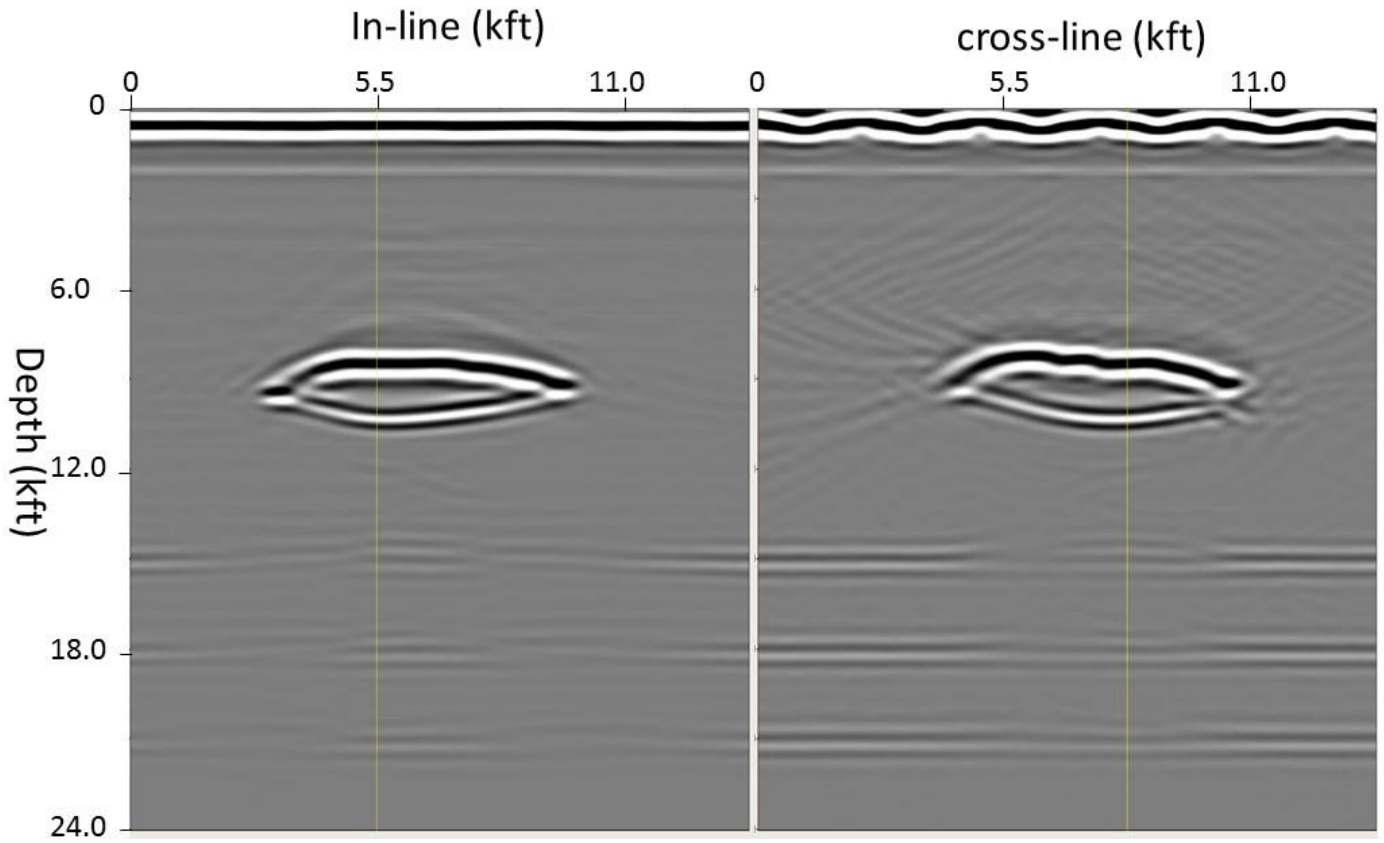

Figure 4.7: 3D RTM image of in-line (left) and cross-line (right) using initial velocity model (Figure 4.8).

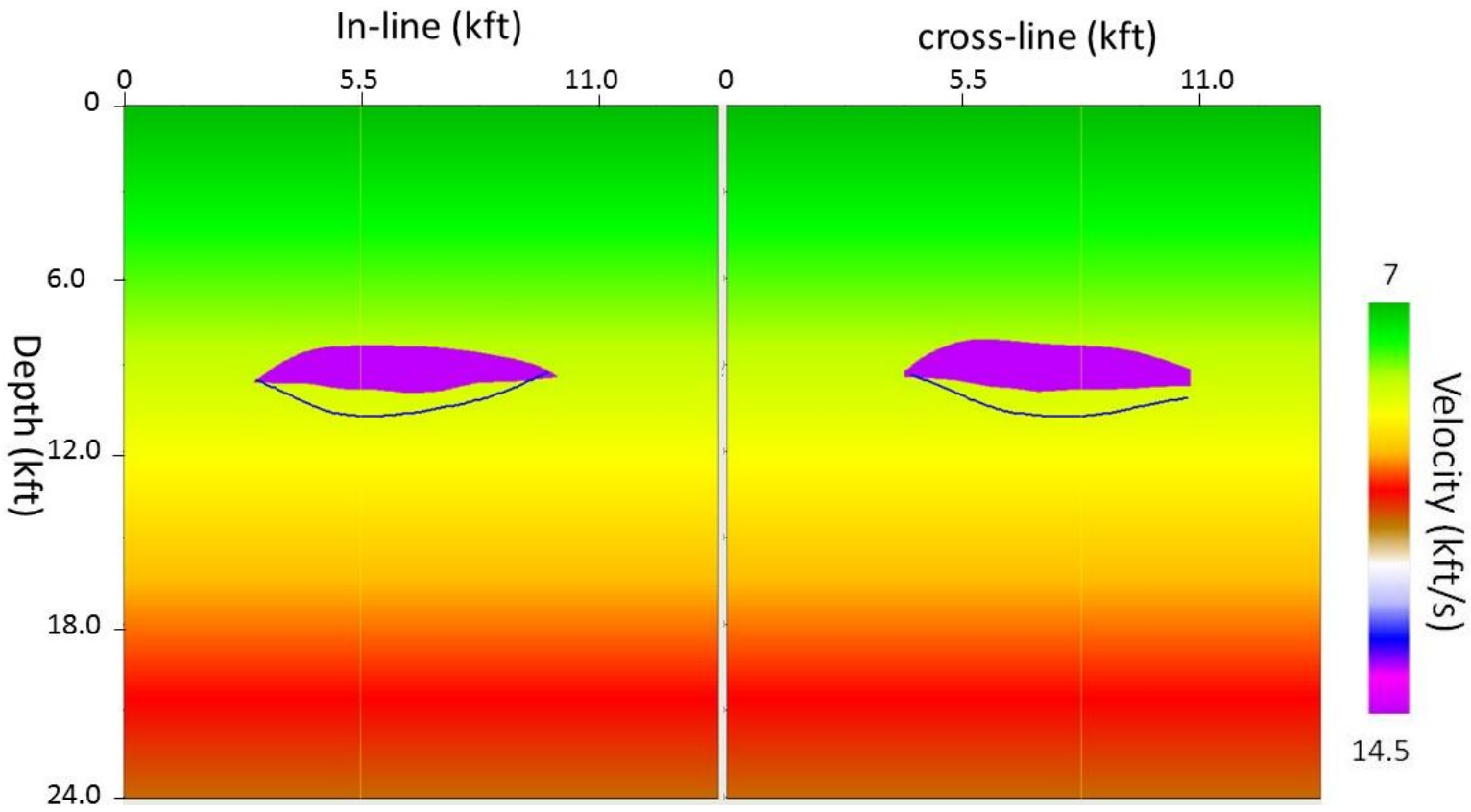

Figure 4.9: First iteration velocity model at in-line (left) and cross-line (right) using 3D RLT. The blue lines show true BOS location.

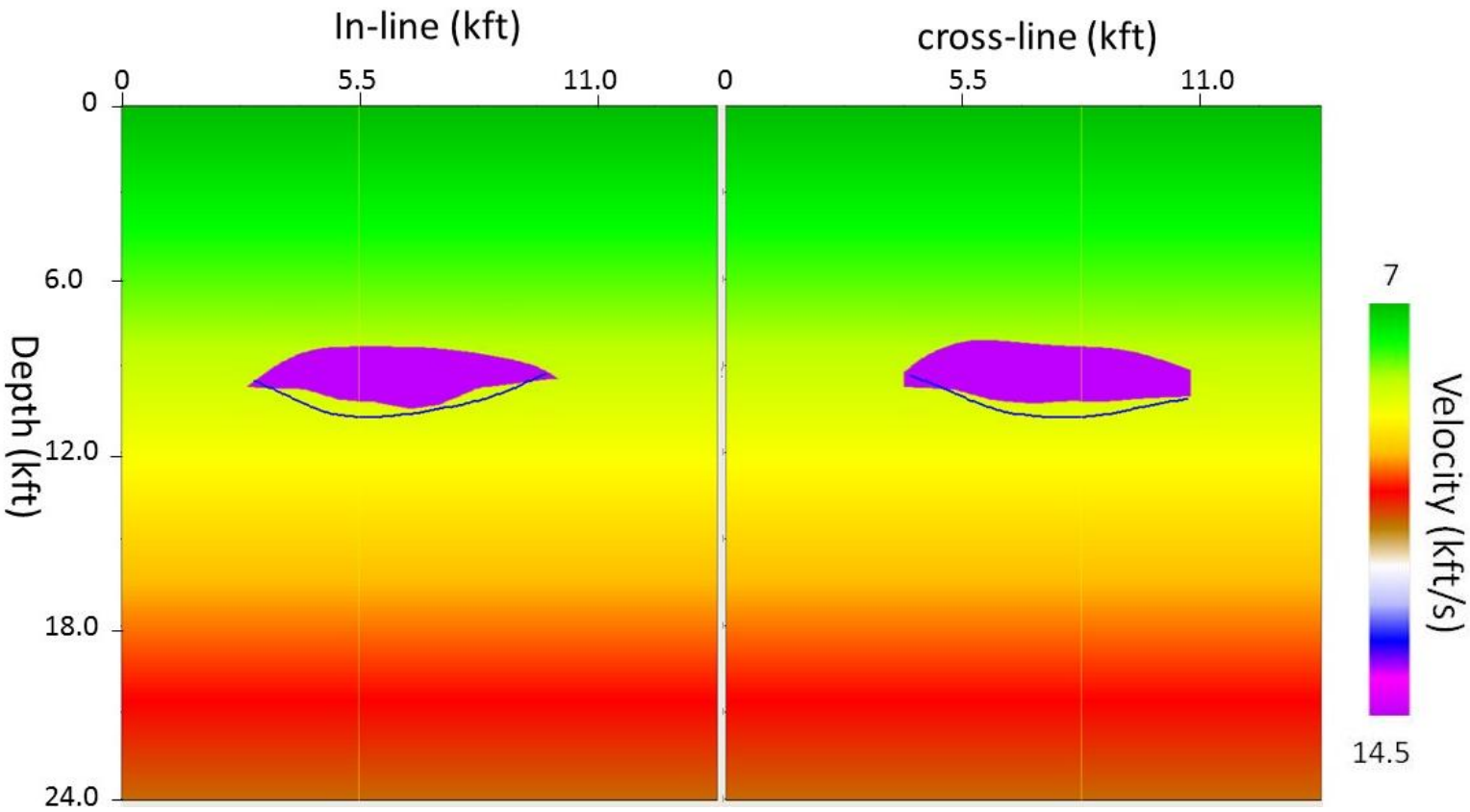

Figure 4.10: Second iteration velocity model at in-line (left) and cross-line (right) using 3D RLT. The blue lines show true BOS location.

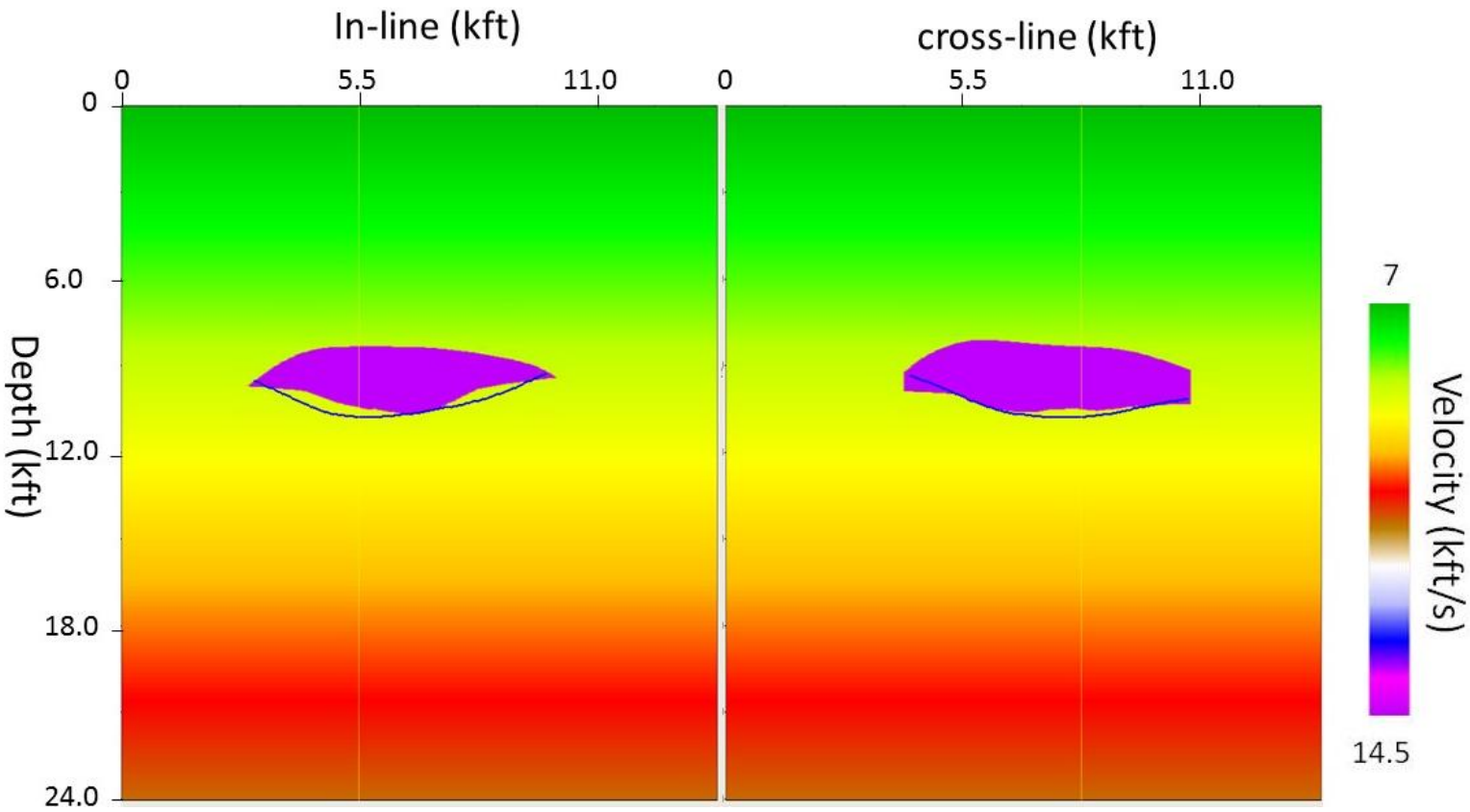

Figure 4.11: Third iteration velocity model at in-line (left) and cross-line (right) using 3D RLT. The blue lines show true BOS location.

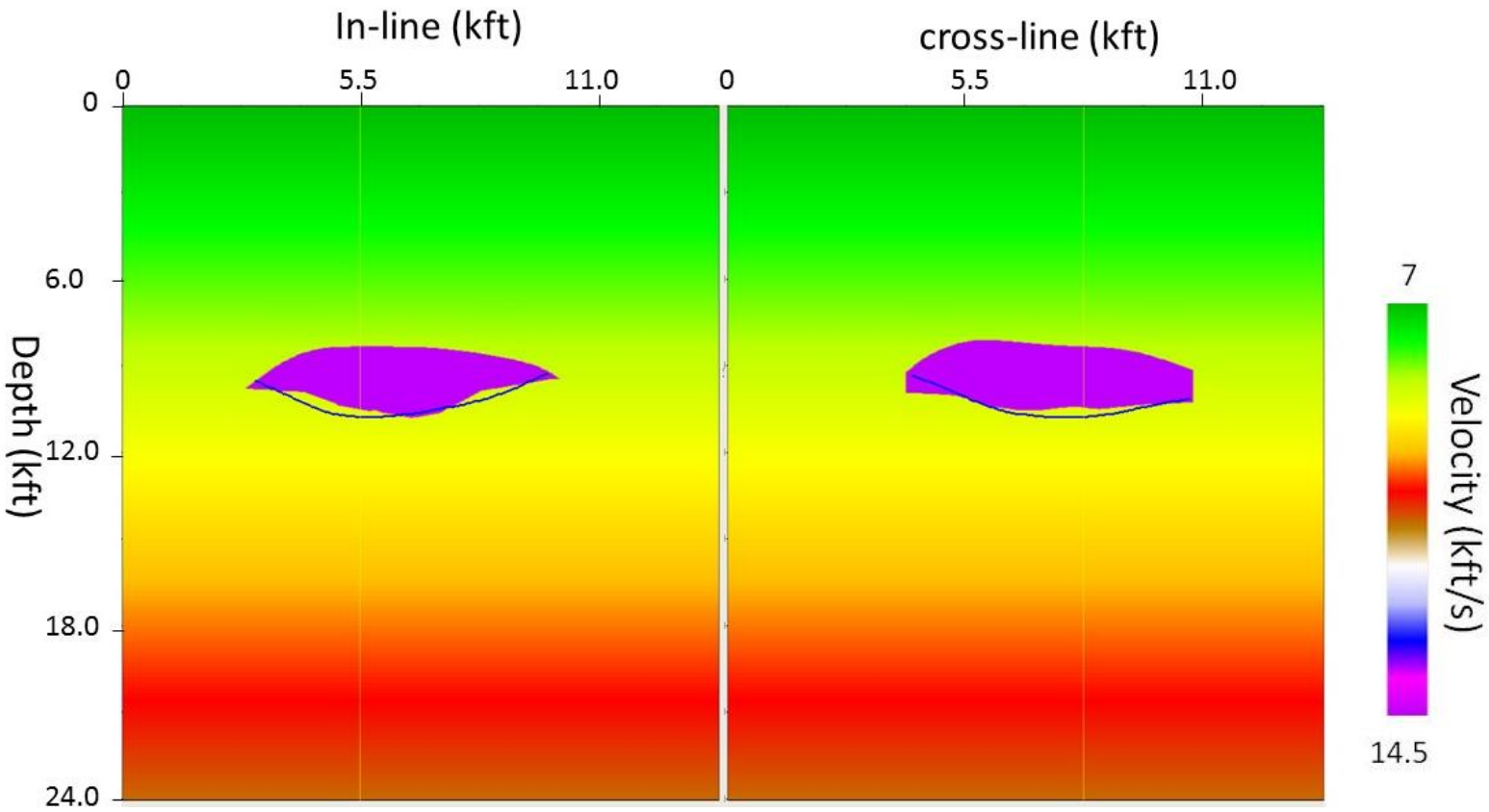

Figure 4.12: Fourth iteration velocity model at in-line (left) and cross-line (right) using 3D RLT. The blue lines show true BOS location.

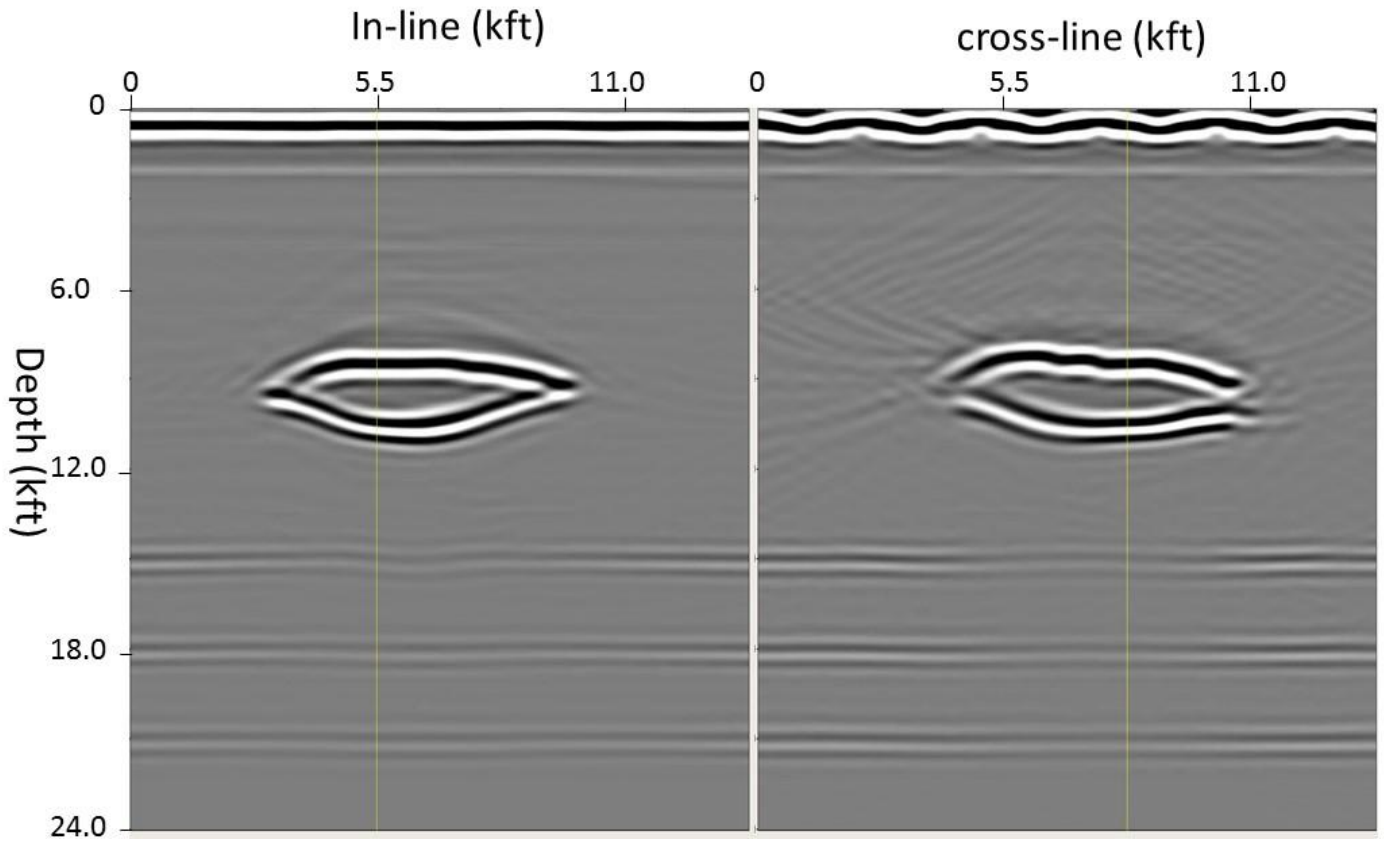

Figure 4.13: RTM image of fourth iteration velocity model at in-line (left) and cross-line (right) .

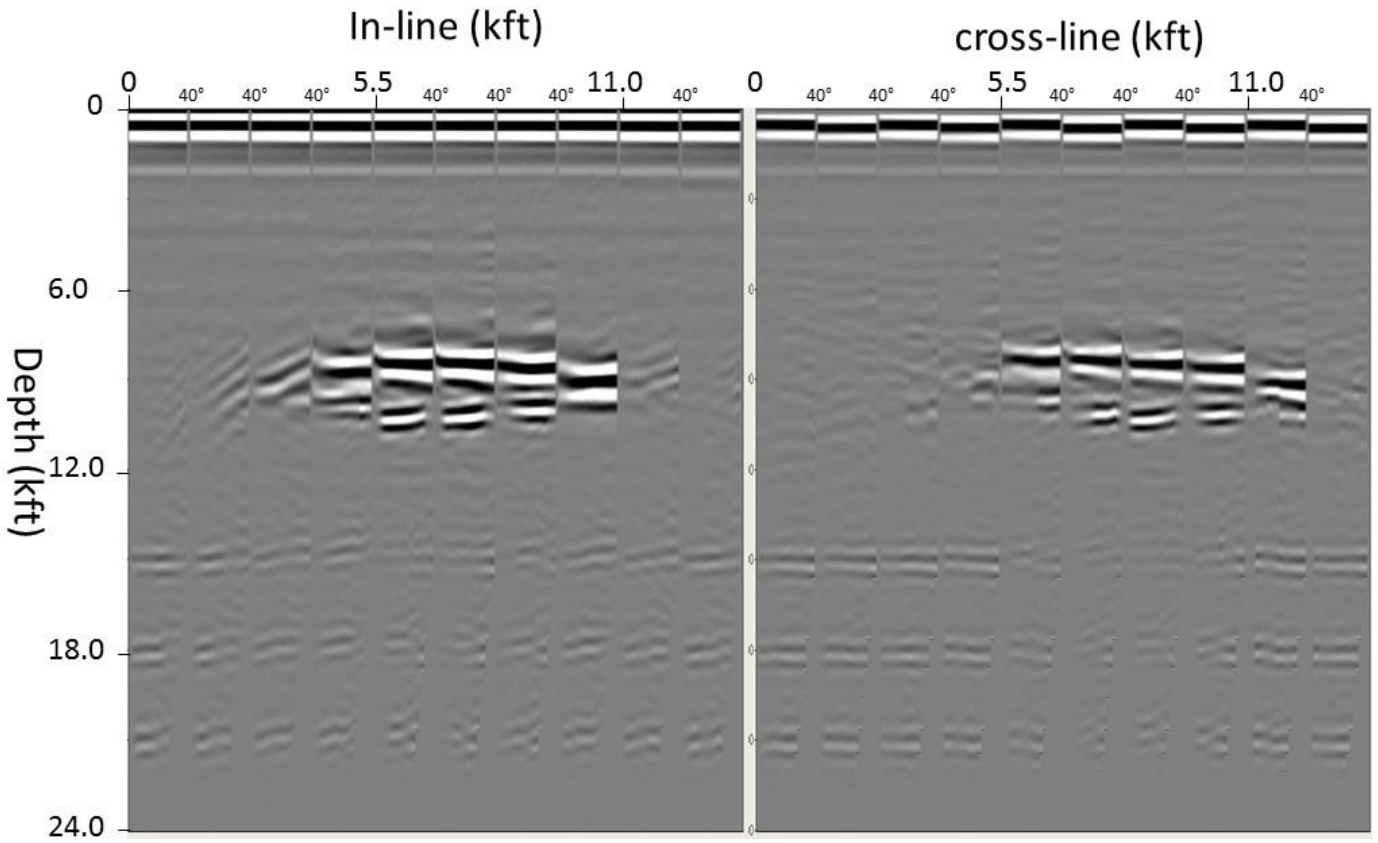

Figure 4.14: ADCIGS of initial mode at in-line (left) and cross-line (right). The maximum angle for each gather is 40°.

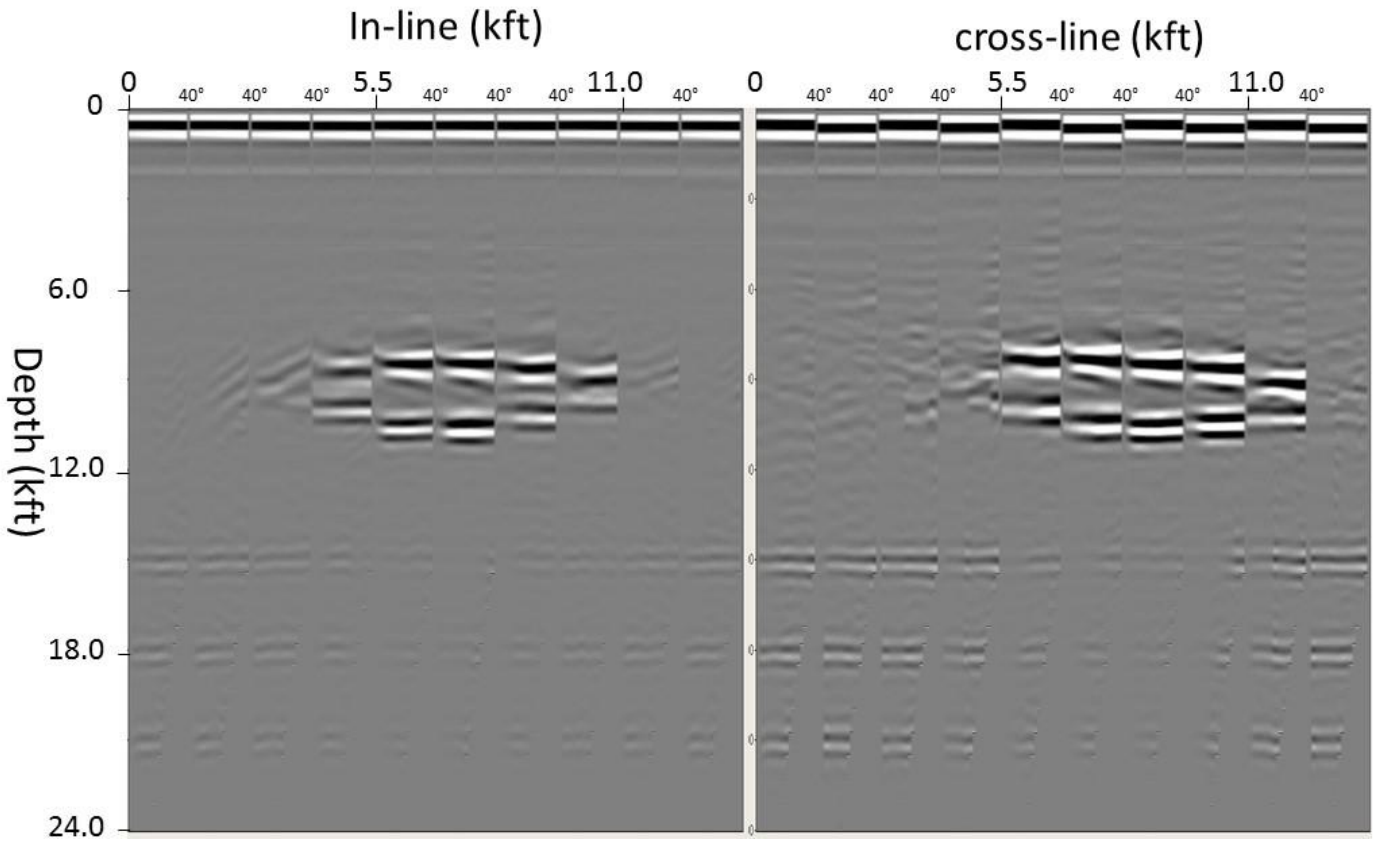

Figure 4.15: ADCIGs of fourth iteration velocity mode at in-line (left) and cross-line (right). The maximum angle for each gather is 40°.

4.4 SUMMARY

RLT have been extended to 3D for practical applications. The synthetic example demonstrates RLT can automatically and effectively estimate the 3D BOS, which expedites the 3D salt model building and the subsequent 3D depth imaging processes. Both RTM stack images and ADCIGs demonstrate 3D RLT can significantly expedite the processes of 3D salt model building and the subsequent depth imaging.

CHAPTER 5: CONCLUSTIONS AND FUTURE WORK

5.1 CONCLUSIONS

In this dissertation, a new and effective reflection layer tomography method is developed for prestack depth migration velocity analysis. This approach provides a significant improvement in automatically estimating the salt boundary. RLT allows us to conduct directly inversion for the depth-varying geometries of velocity discontinuities and to show the velocity structures in a more direct way. RLT take advantage of layer-based tomography to avoid the smearing artifacts on interface generated by grid-based tomography methods. RLT utilizes ADCIGs generated from RTM to eliminate the multi-pathing problem embedded in ODCIGs. The RLT workflow consists of iterative processes of prestack depth migration and tomographic inversion. The application of RLT requires a good overburden velocity model as well as interfaces of top of salt prior to inversion. These two elements can be relatively easily obtained according to standard model building procedures in the industry.

In Chapter 2, a synthetic data set was created to test and validate RLT versatility and accuracy. The synthetic test shows the ability of RLT in effectively and automatically delineating the BOS. The results show that RLT can construct a more accurate salt model and thereby improve the subsalt image. However, due to the uneven picks and poor ray

coverage, it still faces challenges in geologically complex areas, such as for the steep dip salt flanks.

In Chapter 3, a multi-scale strategy is proposed to constrain the base of salt geometry. The multi-scale RLT can handle complex structures, for example, the steep dip salt flanks, where as single-scale RLT may fail to recover the model due to instability and local minima problems caused by insufficient ray coverage. The multi-scale RLT combines different sub-models in different scales. In this way, the multi-scale RLT not only gains high resolution from sub-models of high-wavenumber components, but also stabilizes inversions from sub-models of low-wavenumber components. Compared with the synthetic example of single-scale RLT in Chapter 2, the multi-scale RLT can reduce uncertainties in salt model building, converge faster, and render a more accurate velocity model in complex media, such as the steep dip salt flanks.

In Chapter 4, the RLT is further extended to 3D to make it applicable to real case. The synthetic example demonstrates the applicability of 3D RLT. Both RTM stack images and ADCIGs reveal the significance of the 3D RLT, which can build an accurate salt model for sub-salt imaging. With 3D RLT, one can significantly expedite the processes of 3D salt model building and the subsequent depth imaging.

The assumption of RLT is needed to interpret the model layer prior to inversion and a good overburden velocity, which can be relatively easily realized with standard model

building procedures. Although the synthetic test shows a good probability to invert the interface geometers by using reflection data, field data may bring more challenges, such as irregular acquisition and a poor signal to noise ratio. Moreover, in real applications, the raypath coverage depends not only on the acquisition system, but also on the velocity model. Thus, even with regular spaces, shots, and receivers, ray coverage can be uneven in the heterogeneity model. The issue of depth-velocity ambiguity is ever present with velocity inversion methods. Even with a very simple model, the non-uniqueness still exists in velocity-depth determination. This means that a number of models flattening RMOs can be observed equally well.

5.2 FUTURE WORK

Although the synthetic tests in this study show promising results (for example, a well recovered salt geometry and improved subsalt images), field data applications may still bring more challenges, such as irregular acquisition and poor signal to noise ratio. Moreover, in real applications, the issue of depth-velocity ambiguity is ever present with many velocity analysis methods, meaning that a number of models can satisfy observation equally well and flatten CIGs. To facilitate the application of this study in more realistic examples, some potential research directions for future work are also mentioned as follows:

First, the current RLT approach only updates interface geometry. Further study will be able to induce velocity updates inside layers. The simultaneous inversion of velocities and interfaces could be a useful extension for building dirty salt models. Second, the current RLT approach is based on P-waves delineating the interface geometries; therefore, it will be interesting to use S-waves or converted waves, which could be an encouraging research topic. In addition, the multi-scale strategy, as a basic optimization scheme, could be used to obtain other parameters, such as anisotropic parameters and attenuations, through tomographic inversion.

REFERENCES

Aki, K., A. Christoffersson, E. S. Husebye, 1977, Determination of the three-dimensional seismic structure of the lithosphere: Journal of Geophysical Research, 82, 277–296.

Aki, K. and W. H. K. Lee, 1976, Determination of the three-dimensional velocity anomalies under a seismic array using first P arrival times from local earthquakes 1: A homogeneous initial model: Journal of Geophysical Research, 81, 4381–4399.

Allaud, L. A. and M. H. Martin, 1977, Schlumberger the History of a Technique: New York, New Your, USA: John Wiley & Sons.

Backus, G. and F. Gilbert, 1968, The resolving power of gross earth data: Geophysical Journal of the Royal Astronomical Society, 16, 169-205.

Baysal, E., D. D. Kosloff, and J. W. C. Sherwood, 1983, Reverse-time migration: Geophysics, 48, 1514–1524.

Bickel, S. H., 1990, Velocity-depth ambiguity of reflection traveltimes: Geophysics, 55, 266–276.

Bishop, T. N., K. P. Bube, R. T. Cutler, R. T. Langan, P. L. Love, R. T. Resnick, R. T. Shuey, D. A. Spindler, and H. W. Wyld, 1985, Tomographic determination of velocity and depth in laterally varying media: Geophysics, 50, 903–923.

Biondi, B., 2006, Prestack exploding-reflectors modeling for migration velocity analysis:

SEG Technical Program Expanded Abstracts, 3056–3060.

Biondi, B. and W. Symes, 2004. Angle-domain common-image gathers for migration velocity analysis by wavefield-continuation imaging. Geophysics, 69, 1283–1298.

Bleistein, N., and S. H. Gray, 2002, A proposal for common-opening-angle migration/inversion: Center for Wave Phenomena Research Report number CWP-420

Bois, P., M. La Porte, M. Lavergne, G. Thomas, 1972, Well-to-well seismic measurements: Geophysics 37, 471–480.

Claerbout, J. F., 1985, Imaging the Earth's interior, Blackwell Scientific Publications, Inc.

Gardner, L. W., 1949, Seismograph determination of salt dome boundary using well detector deep on dome flank: Geophysics, 14, 29-38.

Guiziou, J. L., J. L. Mallet, and R. Madariaga, 1996, 3-D seismic reflection tomography on top of the GOCAD depth modeler: Geophysics, 61, 1499–1510.

Jones, I., M. C. Goodwin, I. D. Berranger, H. Zhou, P. A. Farme, 2007, Application of anisotropic 3D reverse time migration to complex North Sea imaging: 77th Annual International Meeting, SEG, Expanded Abstracts, 2140–2143.

Kosloff, D., J. Sherwood, Z. Koren, E. Machet, and Y. Falkovitz, 1996, Velocity and interfaces depth determination by tomography of depth migrated gathers: Geophysics, 61, 1511-1523.

Leveille, J., K. Larner, and J. Higginbotham, 2005, A problem workshop: The Leading Edge, 24, 1126-1132,

Leveille, J., I. Jones, Z. Zhou, B. Wang, and F. Liu, 2011, Subsalt imaging for exploration, production, and development: A review: Geophysics, 76, WB3–WB20.

Lin, T. 1991, Modeling and imaging of salt dome structures: 61st Annual International Meeting, SEG, Expanded Abstracts, 199-202.

Liu, W., Y. Wang, 2008, Target-oriented reverse time migration for two-way prestack depth imaging: 79th Annual International Meeting, SEG, Expanded Abstracts, 2326–2330.

Lines, L., 1993, Ambiguity in analysis of velocity and depth: Geophysics, 58, 596–597.

Lohmann. H. H., 1979, Seismic recognition of salt diapirs: American Associate of Petroleum Geologists Bulletin, 63, 2097-2102.

Ma, Y., D. Hale, Z. Meng, B. Gong, 2012, Image-guided sparse-model full waveform inversion: Geophysics 77, R189-R198,

May, B. T., J. D. Covey, 1983, Structural inversion of salt dome flanks: Geophysics, 48, 1039-1050.

McMechan, G. A., 1983, Migration by extrapolation of time-dependent boundary values: Geophysical Prospecting, 31, 413–420.

Meng, Z., P. A. Valasek, S. A. Whitney, C. B. Sigler, B. K. Macy and N. Dan Whitmore, 2004, 3D global tomographic velocity model building: 74th Annual International Meeting, SEG, Expanded Abstracts, 2379-2382.

Mosher, C., E. Keskula, J. Malloy, R. Keys, H. Zhang, and S. Jin, 2007, Iterative imaging for subsalt interpretation and model building: The Leading Edge, 26, 1424–1428.

Reasnor, M. D., 2007, Salt interpretation practices for depth imaging in the Gulf of Mexico: The Leading Edge, 26, 1438–1441.

Sayers, C., and D. Herron, 2007, Introduction to this special section: Subsalt exploration: The Leading Edge, 26, 1404–1405.

Stork, C., 1992, Reflection tomography for the post-migrated domain: Geophysics, 57, 680-692.

Stork, C. and R. W. Clayton, 1991, Linear aspects of tomographic velocity analysis: Geophysics, 56, 483-495.

Wang, B., K. Pann, and R. A. Meek, 1995, Macro velocity model estimation through model based globally-optimized residual-curvature analysis: 65th Annual International Meeting, SEG, Expanded Abstracts, 1084–1087.

Wang, B., Y. Kim, C. Mason, X. Zeng, 2008. Advances in velocity model-building technology for subsalt imaging: Geophysics 73, VE173–VE181.

Wang X. and I. Tsvankin, 2012, Ray-based gridded tomography for tilted transversely isotropic media: Geophysics, 78, C11-C23.

Whitmore, D., 1983, Iterative depth migration by backward time propagation: 53rd Annual International Meeting, SEG, Expanded Abstracts, 382–385.

Woodward M. J., D. Nichols, O. Zdraveva, P. Whitfield, and T. Johns，2008， A decade of tomography: Geophysics, 73, VE5–VE11.

Xu, S., H. Chauris, G. Lambare, M. Noble, 2001, Common-angle migration: a strategy for imaging complex media: Geophysics, 66, 1877–1894.

Yoon, K. and K. J. Marfurt, 2006, Reverse-time migration using the Poynting vector: Exploration Geophysics, 37, 102–107.

Yoon, K., B. Wang, Y. Kim, and H. Guan, 2008, Localized reverse time migration for salt model building: 78th Annual International Meeting, SEG, Expanded Abstracts, 2331–2335.

Zhou, H., 1996, A high-resolution P wave model for top 1200 km of the mantle: Journal Geophysical Research, 101, 27791–27810.

Zhou, H., 2003, Multiscale traveltime tomography: Geophysics, 68, 1639–1649.

Zhou, H., 2006, Multiscale deformable-layer tomography: Geophysics, 71, R11–R19.

Zhou, H., Practical seismic data analysis: 2013, Cambridge.

Zhou, H., H. Liu, F. Jiang, and P. Li, 2008, First-break deformable-layer tomostatics constrained by shallow reflections: 78thAnnualMeeting, SEG, Expanded Abstracts, 3224–3228.